AIP | Physics of Fluids

Surfactant-driven dynamics of liquid lenses

George Karapetsas, Richard V. Craster, and Omar K. Matar

Citation: Phys. Fluids **23**, 122106 (2011); doi: 10.1063/1.3670009
View online: http://dx.doi.org/10.1063/1.3670009
View Table of Contents: http://pof.aip.org/resource/1/PHFLE6/v23/i12
Published by the American Institute of Physics.

Related Articles

Spontaneous mode-selection in the self-propelled motion of a solid/liquid composite driven by interfacial instability
J. Chem. Phys. 134, 114704 (2011)

The effect of confinement-induced shear on drop deformation and breakup in microfluidic extensional flows
Phys. Fluids 23, 022004 (2011)

Influence of surfactant on drop deformation in an electric field
Phys. Fluids 22, 112104 (2010)

Effect of soluble surfactants on dynamic wetting of flexible substrates: A finite element study
Phys. Fluids 21, 122103 (2009)

Influence of surfactant solubility on the deformation and breakup of a bubble or capillary jet in a viscous fluid
Phys. Fluids 21, 072105 (2009)

Additional information on Phys. Fluids

Journal Homepage: http://pof.aip.org/
Journal Information: http://pof.aip.org/about/about_the_journal
Top downloads: http://pof.aip.org/features/most_downloaded
Information for Authors: http://pof.aip.org/authors

ADVERTISEMENT

Downloaded 22 Dec 2011 to 129.31.211.195. Redistribution subject to AIP license or copyright; see http://pof.aip.org/about/rights_and_permissions

Surfactant-driven dynamics of liquid lenses

George Karapetsas,[1] Richard V. Craster,[2] and Omar K. Matar[1,a)]
[1]*Department of Chemical Engineering, Imperial College London, South Kensington Campus, London SW7 2AZ, United Kingdom*
[2]*Department of Mathematics, Imperial College London, South Kensington Campus, London SW7 2AZ, United Kingdom*

(Received 18 March 2011; accepted 7 November 2011; published online 22 December 2011)

Sessile liquid lenses spreading over a fluid layer, in the presence of Marangoni stresses due to surfactants, show a surprisingly wide range of interesting behaviour ranging from complete spreading of the lens, to spreading followed by retraction, to sustained pulsating oscillations. Models for the spreading process, the effects of surfactant at the moving contact line, sorption kinetics above and below the critical micelle concentration, are all incorporated into the modelling. Numerical results cast light upon the physical processes that drive these phenomena, and the regular oscillatory beating of lenses is shown to occur in specific limits. © *2011 American Institute of Physics*. [doi:10.1063/1.3670009]

I. INTRODUCTION

The spreading of liquids on other immiscible liquids is central to a number of applications including coating flow and lubrication technologies, the production of pesticides, fire extinguishing, and anti-foaming agents, oil recovery, and oil-spill clean-up. It is unsurprising, therefore, that this system has been the subject of a number of studies in the literature. The early papers focused mainly on uncontaminated liquids, a prime example of which is the work of Harkins[1] who advanced the concept of a *spreading coefficient*. For the case of a layer of liquid "2" spreading over another immiscible liquid "1," S^* is defined as follows:

$$S^* = \sigma_{13}^* - (\sigma_{23}^* + \sigma_{12}^*). \tag{1.1}$$

Here, σ_{13}^*, σ_{23}^*, and σ_{12}^* denote the surface tension of liquid "1," liquid "2," and of the interface separating these liquids. The superscript "*" indicates that the corresponding variable is dimensional. Spontaneous spreading is expected for $S^* > 0$ and for $S^* < 0$, one expects the formation of a stable lens-shaped drop of liquid "2" on the surface of liquid "1."

The consequences of a positive spreading coefficient, $S^* > 0$, have been studied in several papers[2–5] examining spreading over deep layers for which the spreading exhibits a power-law behaviour, consistent with the scaling theory of Hoult;[6] the radius of a spreading lens, R, scales as $R \sim t^{3/4}$, where t denotes the time elapsed following the deposition of the lens. This scaling is also valid for spreading along the liquid-liquid interface of two deep immiscible fluids.[7] For spreading over thin fluid layers, where the lubrication approximation is valid, the power-law exponent decreases to 1/7.[8,9]

For negative spreading coefficients, $S^* < 0$, Kriegsmann and Miksis[10] studied the steady-state shapes of lenses of one liquid on the surface of another, resting on an inclined plane, using lubrication theory. These authors treated the three-phase contact line as a massless point and derived boundary conditions at this point by writing down equilibrium force balances. More recently, Craster and Matar[11] also used the lubrication approximation to model lens formation but did not consider the presence of the three-phase contact line explicitly. Instead, they followed the approach of Schwartz and Eley[12] and carried out a force balance in the vicinity of the contact line where the lens adjusts onto a thin, stable wetting layer, stabilised by antagonistic intermolecular forces. Craster and Matar[11] used their model to simulate the development of lenses over a wide range of parameters, which included the density, viscosity, and surface tension ratios; they also examined briefly the role of extensional stresses in the lens, which becomes significant for highly viscous lenses.

In addition, a number of papers have examined the effect of surfactants on liquid-on-liquid spreading. Surfactant plays a potentially major role in the spreading process since it can lower significantly the surface tension of the interface upon which it is deposited; gradients in the surfactant interfacial concentration create Marangoni stresses that drive spreading in the direction of higher tension.[13] Surfactants are often present at interfaces in the form of contaminants, or by design, as in the case of detergents; surfactants can also be present naturally, as is the case with phospholipids, an example of lung surfactant, or may be the product of interfacial chemical reactions.[14] Inspection of Eq. (1.1) reveals that surfactants can lower σ_{23}^* and/or σ_{12}^* leading to $S^* > 0$ in situations which would have otherwise been characterised by negative S^*. Bergeron and Langevin[15] showed that similar power-law exponents to those observed for pure liquid can be found in situations, wherein the surfactant is insoluble in the spreading liquid. In other studies, a power-law of $R \sim t^{1/2}$ was observed for the spreading of surfactant solutions on an immiscible organic substrate layer.[16–23] The power-law exponents found by Svitova *et al.*[21] to be consistently lower than the 3/4 predicted by Hoult[6] were attributed by Chauhan *et al.*[22] to the influence of surfactant diffusion within the lens.

The dynamics of lenses containing surfactant are often accompanied by complex behaviour an exemplar of which is the regular oscillatory beating of a sessile lens upon a fluid

a)Author to whom correspondence should be addressed. Electronic mail: o.matar@imperial.ac.uk.

 © 2011 American Institute of Physics

Downloaded 22 Dec 2011 to 129.31.211.195. Redistribution subject to AIP license or copyright; see http://pof.aip.org/about/rights_and_permissions

layer. Experiments by Stocker and Bush,[24] who revisit earlier work by Sebba,[25] show that a surfactant-laden oil drop placed on a water surface has a radius that can oscillate for long times. The long-term sustained oscillatory behaviour is, at first sight, perplexing as one naturally wonders how this behaviour is generated, and sustained, with no obvious source of forcing. Using very careful experiments and video-microscopy, Stocker and Bush[24] reveal that the oscillations are generated by partial emulsification at the lens edge and sustained by the evaporation of surfactant from the water surface. The subsequent retraction of the lens is initiated by the rapid formation of thin films at the lens leading edge, due to growth of perturbations in the azimuthal direction, releasing surfactant at the water-air interface, and thereby decreasing its surface tension. This provides a serious challenge in terms of modelling; a model for the lens oscillations is developed in Sec. IV B 4.

In spite of these numerous studies in the literature, the spreading behaviour of surfactant-laden lenses remains poorly understood. To the best of our knowledge, we are not aware of any models capable of providing accurate predictions of the dynamics of surfactant-laden lenses of one liquid spreading on the surface of another immiscible liquid. We therefore revisit this problem, our aim being to create models of sufficient complexity that they are capable of capturing observed phenomena, but are sufficiently simple so as to allow for physical interpretation; the fluid mechanics takes advantage of the thin lenses and consider flow over a shallow layer, thereby allowing the lubrication approximation to be utilized. We build on the work of Karapetsas *et al.*,[26] who studied the super-spreading of thin surfactant-laden drops on solid substrates,[27,28] and derive a coupled set of equations for the interfaces "13," "23," and "12" [as defined by Eq. (1)], and for the surfactant concentrations at these interfaces. The surfactant is allowed to exist in the form of interfacial and bulk monomers, as well as in the form of micellar aggregates. The model developed accounts for Marangoni stresses, surface and bulk diffusion, sorption and micellar formation and breakup kinetics, and the effects of surfactant on the moving contact line. Our results demonstrate that power-law exponents range from 1/7 to 1/2 depending on the range of parameters investigated. We also show that it is possible, under certain conditions, for the lens to exhibit sustained oscillations reminiscent of those observed by Stocker and Bush;[24] the mechanism underlying this behaviour is detailed herein.

The rest of the paper is organised as follows. Details of the model derivation and of the numerical procedure are provided in Secs. II and III, respectively. A discussion of the results of our parametric study can be found in Sec. IV; this section also contains details of the numerical procedure used to carry out the computations. Finally, concluding remarks are given in Sec. V.

II. PROBLEM FORMULATION

The dynamics of a surfactant-laden lens of a viscous fluid of density ρ_2^* and viscosity μ_2^* spreading on the surface of a layer of another fluid of density and viscosity ρ_1^* and μ_1^*, respectively, is considered; properties of the lens and of the bottom fluid will, henceforth, be designated by subscripts 1 and 2, respectively. Both fluids are assumed to be incompressible, Newtonian, and immiscible. The bottom layer is bounded from below by an impermeable, rigid, and horizontal solid substrate, while both fluids are bounded from above by an essentially inviscid gas (designated by subscript 3). The surface tensions of the lens-air, substrate-air, and lens-substrate interfaces are σ_{13}^*, σ_{23}^*, and σ_{12}^*, respectively. We assume that initially the lens has a half-width L^* and volume V_2^* as shown in Fig. 1. In the present work, we consider the drop to be very thin so that the drop aspect ratio, $\varepsilon = V_2^*/L^{*2}$, is assumed to be very small; this is a reasonable assumption for the majority of experimental situations of, say, oil spreading upon water. This assumption permits the use of lubrication theory, which will be employed below to derive a set of evolution equations that govern the spreading process. It should be noted here that the lubrication approximation assumes small slopes, and therefore, this model does not formally capture droplet spreading with high contact angles. Our primary interest is in developing a model, sufficiently complicated to capture the essential physics, whilst being simple enough to isolate and understand the physicochemical mechanisms primarily at the droplet edge, and hence, we consider Cartesian rather than axisymmetric, model geometry.

A. Hydrodynamics

We use a Cartesian coordinate system, (x^*, z^*), to model the dynamics, and the velocity field is $\underline{u}^* = (u^*, w^*)$, where u^* and w^* correspond to the horizontal and vertical components of the velocity field, respectively. The various interfaces are located at $z^* = h_j^*(x^*, t^*)$, where $j = 12, 13, 23$. The spreading dynamics for both fluids are governed by momentum and mass conservation equations, respectively, given below

$$\rho_i^*\left(\underline{u}_{i,t^*}^* + \underline{u}_i^* \cdot \underline{\nabla}\underline{u}_i^*\right) + \underline{\nabla} p_i^* - \mu_i^* \nabla^2 \underline{u}_i^* - \rho_i^* \underline{g}^* = 0, \quad (2.1)$$

$$\underline{\nabla} \cdot \underline{u}_i^* = 0, \quad i = 1, 2, \quad (2.2)$$

where $\underline{u}_i^*$, p_i^*, $\underline{g}^*$ are the velocity vector, pressure, and gravitational acceleration, respectively, while $\underline{\nabla}$ denotes the gradient operator. Unless stated otherwise, the subscripts denote

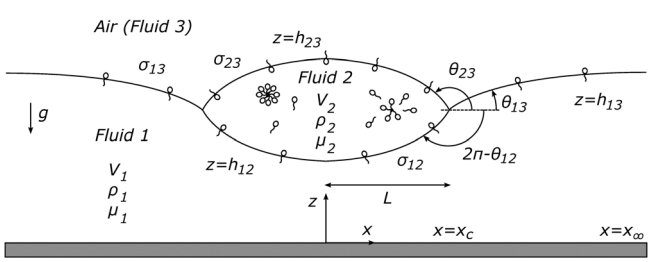

FIG. 1. A schematic of a two-dimensional lens of fluid 2 of volume V_2 and half-width L, spreading over fluid 1 of volume V_1. The surfactant is soluble in fluid 2 and insoluble in fluid 1, and it can be present in the bulk of the lens as monomers or aggregates such as micelles or vesicles, and at all the interfaces as monomers.

Downloaded 22 Dec 2011 to 129.31.211.195. Redistribution subject to AIP license or copyright; see http://pof.aip.org/about/rights_and_permissions

partial differentiation with respect to x^*, z^*, and t^*, where t^* denotes time.

Solutions of Eqs. (2.1) and (2.2) are obtained subject to the following boundary conditions. Along the interfaces, the velocity field should satisfy a local force balance between surface tension and viscous stresses in the neighboring fluids. Setting the pressure in the surrounding gas to zero (datum pressure), without loss of generality, we obtain

$$\underline{n}_j \cdot \underline{\underline{T_2}}^* = \underline{\nabla}_{s,j}\sigma_j^* + 2\underline{n}_j\kappa_j^*\sigma_j^*, \quad j = 13, 23, \tag{2.3}$$

$$\underline{n}_{12} \cdot \underline{\underline{T_1}}^* - \underline{n}_{12} \cdot \underline{\underline{T_2}}^* = \underline{\nabla}_{s,12}\sigma_{12}^* + 2\underline{n}_{12}\kappa_{12}^*\sigma_{12}^*, \tag{2.4}$$

where $\underline{n}_j = \left(-h_{j,x^*}^*, 1\right)\Big/\left(1 + h_{j,x^*}^{*\,2}\right)^{1/2}$ denote the outward unit normal on the interface j, $\underline{\nabla}_{s,j}$ is the corresponding surface gradient operator, and $\underline{\underline{T_i}}^*$ is the total stress tensor in fluid i given by

$$\underline{\underline{T_i}}^* = -p_i^*\underline{\underline{I}} + \mu_i^*\left[\underline{\nabla}\underline{u}_i^* + \left(\underline{\nabla}\underline{u}_i^*\right)^T\right], \tag{2.5}$$

where $\underline{\underline{I}}$ is the identity tensor and $2\kappa_j^*$ is the mean curvature of the interface j, defined as

$$2\kappa_j^* = -\underline{\nabla}_{s,j} \cdot \underline{n}_j, \quad \underline{\nabla}_{s,j} = \left(\underline{\underline{I}} - \underline{n}_j\underline{n}_j\right) \cdot \underline{\nabla}. \tag{2.6}$$

In addition, along the moving interfaces, we apply the kinematic boundary condition,

$$h_{j,t^*}^* + u_{s,j}^* h_{j,x^*}^* = w_{s,j}^*, \text{ at } z^* = h_j^*(x^*, t^*), \tag{2.7}$$

where $u_{s,j}^*$ and $w_{s,j}^*$ are the surface velocities at interface j.

At the liquid-solid interface, the usual no-slip, no-penetration conditions are imposed,

$$u_1^* = 0, \quad w_1^* = 0. \tag{2.8}$$

B. Surfactant transport and chemical kinetics

We utilize the surfactant kinetic model of Edmonstone *et al.*[29] and Karapetsas *et al.*[26] that allows for two surfactant species in the bulk (bulk monomers and micelle aggregates) and one at each interface; when the bulk monomer concentration is such that the bulk concentration of monomers in the lens is above the critical micelle concentration, c_{cmc}^*, then it is energetically favorable for the monomers to form micelles. We assume that, below the c_{cmc}^*, the surfactant exists in the form of monomers within the bulk with concentration c_2^*, whereas, beyond the c_{cmc}^*, micellar aggregates are formed with concentration m_2^*. The various surfactant species interact according to the following kinetic laws. First, at both interfaces of the lens, the transfer of surface monomers, c_{23}^*, into the bulk phase, c_2^*, creates space at the interface or, conversely, monomers from the bulk occupy space at the interface,

$$S_{23} + c_2^* \underset{k_2^*}{\overset{k_1^*}{\rightleftharpoons}} c_{23}^*, \quad S_{12} + c_2^* \underset{k_4^*}{\overset{k_3^*}{\rightleftharpoons}} c_{12}^*, \tag{2.9}$$

where S_j $(j = 12, 23)$ denotes the fraction of the total space created by the desorption of the monomers with concentration c_j^* $(j = 12, 23)$. We note here that our model assumes that there is no direct adsorption of the micelle aggregates at the interfaces; the micelles must disassociate first into monomers before adsorbing at the interface. The micelles and the bulk monomers are related via

$$Nc_2^* \underset{k_6^*}{\overset{k_5^*}{\rightleftharpoons}} m_2^*, \tag{2.10}$$

which represents the creation of a micelle from N bulk monomers or, conversely, the breakup of a micelle into N bulk monomers. We have assumed here that there is a strongly preferred micelle size, N, which is indeed often the case.[30,31] The chemical kinetics are simple enough that modelling can proceed, but still contain the essential physics that allows the model to capture realistic processes. The model can be adjusted to allow for more complicated behaviour, for, say, multiple micelle sizes, at the expense of further evolution equations; indeed the model is not restricted to micelles and could represent any aggregate of N monomers in the bulk.

A key new addition to the kinetic modeling is the behaviour of the surfactant exactly at the contact line; monomers at the interface 23 could be adsorbed directly at the liquid substrate (interfaces 12, 13) through the contact line or vice-versa. This is modelled using the following "reactions":

$$\begin{aligned} &S_{23} + c_{12}^* \underset{k_8^*}{\overset{k_7^*}{\rightleftharpoons}} S_{12} + c_{23}^*, \quad S_{12} + c_{13}^* \underset{k_{10}^*}{\overset{k_9^*}{\rightleftharpoons}} S_{13} + c_{12}^*, \\ &S_{23} + c_{13}^* \underset{k_{12}^*}{\overset{k_{11}^*}{\rightleftharpoons}} S_{13} + c_{23}^*. \end{aligned} \tag{2.11}$$

According to the first "reaction" in Eq. (2.11), the adsorption of surface monomers, c_{23}^*, occupies space at the liquid substrate, S_{12}, creates space, S_{23}, at the liquid-air interface and, conversely, as monomers, c_{12}^*, desorb from the substrate and adsorb at the liquid-air interface. Note that each "reaction" used for this model is characterized by a rate constant k_i^* with $i = 1, 2, ..., 12$. We use these kinetic laws to generate the relevant fluxes that determine how the surfactant transfers between the different phases (see Appendix A).

The behaviour of the various surfactant species is modelled by the following advection-diffusion equations:

$$\begin{aligned} &c_{23,t^*}^* + \underline{\nabla}_{s,23} \cdot \left(\underline{u}_{s,23}^* c_{23}^*\right) + c_{23}^*\left(\underline{\nabla}_{s,23} \cdot \underline{n}_{23}\right)\left(\underline{u}_2^* \cdot \underline{n}_{23}\right) \\ &\quad = D_{23}^* \nabla_{s,23}{}^2 c_{23}^* + J_{c2c23}^* + J_{ev23}^*, \end{aligned} \tag{2.12}$$

$$\begin{aligned} &c_{12,t^*}^* + \underline{\nabla}_{s,12} \cdot \left(\underline{u}_{s,12}^* c_{12}^*\right) + c_{12}^*\left(\underline{\nabla}_{s,12} \cdot \underline{n}_{12}\right)\left(\underline{u}_2^* \cdot \underline{n}_{12}\right) \\ &\quad = D_{12}^* \nabla_{s,12}{}^2 c_{12}^* + J_{c2c12}^*, \end{aligned} \tag{2.13}$$

$$\begin{aligned} &c_{13,t^*}^* + \underline{\nabla}_{s,13} \cdot \left(\underline{u}_{s,13}^* c_{13}^*\right) + c_{13}^*\left(\underline{\nabla}_{s,13} \cdot \underline{n}_{13}\right)\left(\underline{u}_1^* \cdot \underline{n}_{13}\right) \\ &\quad = D_{13}^* \nabla_{s,13}{}^2 c_{13}^* + J_{ev13}, \end{aligned} \tag{2.14}$$

$$c_{2,t^*}^* + \underline{u}_2^* \cdot \underline{\nabla} c_2^* = D_{c2}^* \nabla^2 c_2^* - NJ_2^*, \tag{2.15}$$

$$m_{2,t^*}^* + \underline{u}_2^* \cdot \underline{\nabla} m_2^* = D_{m2}^* \nabla^2 m_2^* + J_2^*, \tag{2.16}$$

where $\underline{u}_{s,j}^*$ is the interfacial velocity defined as

Downloaded 22 Dec 2011 to 129.31.211.195. Redistribution subject to AIP license or copyright; see http://pof.aip.org/about/rights_and_permissions

$$\underline{u}^*_{s,j} = \begin{cases} \left(\underline{\underline{I}} - \underline{n}_j\underline{n}_j\right)\underline{u}^*_2, & j = 23, 12 \\ \left(\underline{\underline{I}} - \underline{n}_j\underline{n}_j\right)\underline{u}^*_1, & j = 13 \end{cases}, \tag{2.17}$$

and D^*_i $(i = 13, 23, 12, c2, m2)$ denote the diffusion coefficients of the monomers at the interfaces, of the monomers in the bulk and the micelles, respectively. We should note here that our model also accounts for the possible "evaporation" of the interfacial surfactant into the atmosphere. To this end, we have used two additional fluxes, $J^*_{ev,j}$ $(j = 13, 23)$, which appear in Eqs. (2.12) and (2.14) and are given by the following relations:

$$J^*_{ev23} = -k^*_{13}c^*_{23}, \quad J^*_{ev13} = -k^*_{14}c^*_{13}. \tag{2.18}$$

Note that the evaporation of the liquid phases is ignored and this assumption is valid only in cases where the surfactant is much more volatile than the rest liquids present in our system. In addition, we ignore the effect of induced temperature gradients due to the surfactant "evaporation" on the surface tension of all interfaces. The latter assumption is valid in cases where the surface tension depends weakly on temperature, or the induced temperature gradients are not significant.

To complete the description of our model, a constitutive equation that describes the dependence of the interfacial tensions on the surfactant concentrations is required. To this end, we use the Sheludko equation of state,[32,33]

$$\sigma^*_j = \sigma^*_{jo}\left(1 + \frac{c^*_j}{c^*_{j\infty}}\left[\left(\frac{\sigma^*_{jo}}{\sigma^*_{jm}}\right)^{1/3} - 1\right]\right)^{-3}, \quad \text{for } j = 13, 23, 12, \tag{2.19}$$

where σ^*_{jo} and σ^*_{jm} $(j = 13, 23, 12)$ are the surface tensions of a surfactant-free fluid and that of maximal surfactant concentration, respectively. This model is nonlinear and asymptotes to a minimal surface tension, σ^*_{jm}, at high concentrations of adsorbed surfactant, which makes it appropriate for use at high surfactant concentrations.

The total mass of the surfactant deposited per unit length, M^*, is a conserved quantity, given by

$$\int_0^{x^*_c}\int_0^{h^*}\left(c^*_2 + Nm^*_2\right)dz^*dx^* + \int_0^{x^*_c}\left(c^*_{23} + c^*_{12}\right)dx^* + \int_{x^*_c}^{x_\infty} c^*_{13}dx^* = M^*, \tag{2.20}$$

where we use symmetry and consider only $x > 0$. Of course, the above equation holds only in the absence of surfactant "evaporation." In the latter case, the mass surfactant present in our system continuously decreases.

C. Scaling

The governing equations and boundary conditions are made dimensionless using the following scalings:

$$\begin{aligned}
&\left(x^*, z^*, h^*_j\right) = L^*\left(x, \varepsilon z, \varepsilon h_j\right), \quad t^* = \frac{L^*}{U^*}t, \quad \left(u^*_i, w^*_i\right) = U^*(u_i, \varepsilon w_i), \quad p^*_i = \frac{\mu^*_1 U^*}{\varepsilon^2 L^*}p_i, \\
&\left(c^*_{13}, c^*_{23}, c^*_{12}\right) = \left(c^*_{13,\infty}c_{13}, c^*_{23,\infty}c_{23}, c^*_{12,\infty}c_{12}\right), \quad \left(c^*_2, m^*_2\right) = c^*_{cmc}(c_2, m_2/N), \\
&\left(J^*_{c2c23}, J^*_{c2c12}, J^*_2, J^*_{ev23}, J^*_{ev13}\right) = \frac{U^*}{L^*}\left(c^*_{23,\infty}J_{c2c23}, c^*_{12,\infty}J_{c2c12}, c^*_{cmc}J_2, c^*_{23,\infty}J_{ev23}, c^*_{13,\infty}J_{ev13}\right), \\
&\left(J^*_{c12c23}, J^*_{c13c12}, J^*_{c13c23}\right) = U^*\left(c^*_{12,\infty}J_{c12c23}, c^*_{13,\infty}J_{c13c12}, c^*_{13,\infty}J_{c13c23}\right), \\
&M^* = V^*_2 c^*_{cmc}M, \quad \sigma^*_j = \sigma^*_{jm} + (\sigma^*_{jo} - \sigma^*_{jm})\sigma_j, \quad (j = 13, 23, 12),
\end{aligned} \tag{2.21}$$

where $U^* = \varepsilon\left(\sigma^*_{23o} - \sigma^*_{23m}\right)/\mu^*_1$ is a characteristic Marangoni velocity, σ^*_{jo} and σ^*_{jm} are the surface tension of zero and maximum surfactant concentration, respectively, and $c^*_{cmc} = \left(\frac{k^*_6}{Nk^*_5}\right)^{\frac{1}{N-1}}$.

Substitution of these scalings into the momentum and mass conservation governing equations and boundary conditions, using the lubrication approximation $(\varepsilon = V^*_2/L^{*2} \ll 1)$, yields a set of reduced equations that are then easily solved. In this process, the following dimensionless groups emerge: $\mu = \mu^*_2/\mu^*_1$, $\rho = \rho^*_2/\rho^*_1$, $Bo = \frac{\varepsilon^3\rho^*_1 g^* L^{*2}}{\mu^*_1 U^*}$, $\delta_j = \sigma^*_{jm}/\sigma^*_{23m}$, and $\Sigma_j = (\sigma^*_{jo} - \sigma^*_{jm})/\sigma^*_{jm}$ $(j = 13, 23, 12)$.

From the kinematic boundary condition and continuity, we obtain

$$h_{j,t} = \begin{cases} -\left(\int_0^{h_j} u_1 dz\right)_x, & j = 12, 13 \\ -\left(\int_0^{h_{12}} u_1 dz + \int_{h_{12}}^{h_{23}} u_2 dz\right)_x, & j = 23 \end{cases}, \tag{2.22}$$

and the velocity integrals are

$$\int_0^{h_{12}} u_1 dz = -\frac{h^3_{12}}{12}p_{1,x} + \frac{h_{12}}{2}u_{s,12}, \tag{2.23}$$

$$\int_{h_{12}}^{h_{23}} u_2 dz = -\frac{(h_{23} - h_{12})^3}{3\mu}p_{2,x} + (h_{23} - h_{12})u_{s,12} + \frac{(h_{23} - h_{12})^2}{2\mu}\sigma_{23,x}, \tag{2.24}$$

$$\int_0^{h_{13}} u_1 dz = -\frac{h^3_{13}}{3}p_{1,x} + \frac{\delta_{13}\Sigma_{13}}{2\Sigma_{23}}h^2_{13}\sigma_{13,x}, \tag{2.25}$$

where the pressure in each fluid is given by

$$p_2 = \rho Boh_{23} - \varepsilon^2 h_{23,xx}(\sigma_{23} + 1/\Sigma_{23}), \tag{2.26}$$

$$p_1 = \begin{cases} (1-\rho)Boh_{12} + p_2 - \varepsilon^2\frac{\delta_{12}}{\Sigma_{23}}(1 + \sigma_{12}\Sigma_{12})h_{12,xx}, & 0 \le x \le x_c \\ Boh_{13} - \varepsilon^2\frac{\delta_{13}}{\Sigma_{23}}(1 + \sigma_{13}\Sigma_{13})h_{13,xx}, & x \ge x_c \end{cases}, \tag{2.27}$$

Downloaded 22 Dec 2011 to 129.31.211.195. Redistribution subject to AIP license or copyright; see http://pof.aip.org/about/rights_and_permissions

and $u_{s,j}$ is the interfacial velocity (at $z = h_j$),

$$u_{s,j} = \begin{cases} h_{12}(h_{23}-h_{12})p_{2,x} - \dfrac{h_{12}^2}{2}p_{1,x} + \dfrac{\delta_{12}\Sigma_{12}}{\Sigma_{23}}h_{12}\sigma_{12,x} + h_{12}\sigma_{23,x}, & , j = 12 \\ -\dfrac{h_{13}^2}{2}p_{1,x} + \dfrac{\delta_{13}\Sigma_{13}}{\Sigma_{23}}h_{13}\sigma_{13,x} & , j = 13\,. \\ u_{s,12} - \dfrac{(h_{23}-h_{12})^2}{2\mu}p_{2,x} + \dfrac{(h_{23}-h_{12})}{\mu}\sigma_{23,x} & , j = 23 \end{cases} \tag{2.28}$$

The dimensionless forms of the Sheludko equation of state for all the interfaces are given by

$$\sigma_j = \left(\frac{1+\Sigma_j}{\Sigma_j}\right)\left(1 + c_j\left[(1+\Sigma_j)^{1/3} - 1\right]\right)^{-3} - \frac{1}{\Sigma_j}, \quad \text{for } j = 12, 13, 23. \tag{2.29}$$

The advection-diffusion equations for the surfactant concentrations, even after using the slender lens assumption (see Appendix B for the scaled equations), have possible variation in depth across the lens and underlying layer, and we adopt one further important simplification.

D. Rapid vertical diffusion

We assume vertical diffusion to be rapid and use an approach previously followed in the literature,[34] that is equivalent to making the following substitution in Eqs. (B1)–(B5):

$$\begin{aligned} c_2(x,z,t) &= c_2^{(0)}(x,t) + \varepsilon^2 Pe_{c2} c_2^{(1)}(x,z,t), \\ m_2(x,z,t) &= m_2^{(0)}(x,t) + \varepsilon^2 Pe_{m2} m_2^{(1)}(x,z,t), \end{aligned} \tag{2.30}$$

and then averaging in the vertical direction of the monomer and micelle equations in the bulk, under the assumption that $\left(\overline{c_2^{(1)}}, \overline{m_2^{(1)}}\right) = \frac{1}{h_{23}-h_{12}}\int_{h_{12}}^{h_{23}}\left(c_2^{(1)}, m_2^{(1)}\right)dz = 0$, taking the limit $\varepsilon^2 Pe_i \to 0$ $(i = c2, m2)$. In addition, we employ the following boundary conditions in the z-direction for the monomers:

$$\begin{aligned} J_{c2c23} &= -\frac{1}{\beta_{c2c23}}\left(-\frac{h_{23,x}}{Pe_{c2}}c_{2,x}^{(0)} + c_{2,z}^{(1)}\right)_{z=h_{23}}, \\ J_{c2c12} &= \frac{1}{\beta_{c2c12}}\left(-\frac{h_{12,x}}{Pe_{c2}}c_{2,x}^{(0)} + c_{2,z}^{(1)}\right)_{z=h_{12}}, \end{aligned} \tag{2.31}$$

which are the dimensionless form of Eqs. (A1) and (A2), as well as the ones for the micelles,

$$m_{2,z}^{(1)}\Big|_{z=h_{23}} = m_{2,z}^{(1)}\Big|_{z=h_{12}} = 0, \tag{2.32}$$

since, as was mentioned above, we assume that there is no direct adsorption of micelles at the liquid-air interface or the substrate. The dimensionless parameters β_{c2c23} and β_{c2c12} provide a measure of surfactant solubility in the bulk fluid and are given by

$$\beta_{c2c23} = \frac{c_{23,\infty}^*}{\varepsilon L^* c_{cmc}^*}, \quad \beta_{c2c12} = \frac{c_{12,\infty}^*}{\varepsilon L^* c_{cmc}^*}. \tag{2.33}$$

After dropping the "(0)" and "(1)" decoration, we obtain the following equations:

$$c_{23,t} + \left(u_{s,23}c_{23}\right)_x = \frac{c_{23,xx}}{Pe_{23}} + J_{c2c23} + J_{ev23}, \tag{2.34}$$

$$c_{12,t} + \left(u_{s,12}c_{12}\right)_x = \frac{c_{12,xx}}{Pe_{12}} + J_{c2c12}, \tag{2.35}$$

$$c_{13,t} + \left(u_{s,13}c_{13}\right)_x = \frac{c_{13,xx}}{Pe_{13}} + J_{ev13}, \tag{2.36}$$

$$c_{2,t} + \frac{c_{2,x}}{(h_{23}-h_{12})}\int_{h_{12}}^{h_{23}} u_2 dz = \frac{\left[(h_{23}-h_{12})c_{2,x}\right]_x}{(h_{23}-h_{12})Pe_{c2}} - \frac{\beta_{c2c23}}{h_{23}-h_{12}}J_{c2c23} - \frac{\beta_{c2c12}}{h_{23}-h_{12}}J_{c2c12} - J_2, \tag{2.37}$$

$$m_{2,t} + \frac{m_{2,x}}{(h_{23}-h_{12})}\int_{h_{12}}^{h_{23}} u_2 dz = \frac{\left[(h_{23}-h_{12})m_{2,x}\right]_x}{(h_{23}-h_{12})Pe_{m2}} + J_2. \tag{2.38}$$

The dimensionless form of the fluxes in the above equations are given in Appendix B.

Finally, the total dimensionless mass of surfactant is given by

$$\int_0^{x_c}(h_{23}-h_{12})(c_2+m_2)dx + \beta_{c2c23}\int_0^{x_c} c_{23}dx + \beta_{c2c12}\int_0^{x_c} c_{12}dx + \beta_{c2c13}\int_{x_c}^{x_\infty} c_{13}dx = M. \tag{2.39}$$

III. NUMERICAL METHOD

A. Finite element method

The discretization of the governing equations is performed using a finite element/Galerkin method, and we approximate all the variables using quadratic Lagrangian basis functions, ϕ^i; it is numerically convenient to decompose each fourth order partial differential equation into two second order differential equations. Appendix C contains the detailed weak formulation equations used in our numerical algorithms. The details on how we map the physical domain onto a computational one are presented in Appendix D.

B. Boundary conditions

To solve the above set of equations, we need to impose appropriate boundary equations in the x-direction, which are applied by substituting the boundary terms in

Downloaded 22 Dec 2011 to 129.31.211.195. Redistribution subject to AIP license or copyright; see http://pof.aip.org/about/rights_and_permissions

Eqs. (C1)–(C11). At the plane of symmetry, we apply symmetry conditions

$$h_{j,x} = h_{j,xxx} = 0 \text{ and } c_{j,x} = c_{2,x} = m_{2,x} = 0 \text{ at } x = 0 \ (j = 12, 23). \tag{3.1}$$

We expect that, very far from the drop, the fluid velocity should be zero, whilst the interfacial surfactant concentration should not be affected by the presence of the drop; thus, we impose

$$h_{13,x} = h_{13,xxx} = 0 \text{ and } c_{13,x} = 0 \text{ at } x = x_\infty. \tag{3.2}$$

1. Contact line

The modeling at the contact line is essential as the physicochemical processes at this point are crucial to the lens behaviour. At the contact line, we impose the continuity of the interfaces

$$h_{23} = h_{13} \text{ and } h_{12} = h_{13} \text{ at } x = x_c. \tag{3.3}$$

Moreover, the pressure in fluid 1 should be continuous at $x = x_c$, which results in the following relation:

$$h_{23,xx}(1 + \Sigma_{23}\sigma_{23}) + h_{12,xx}(1 + \Sigma_{12}\sigma_{12})\delta_{12} - h_{13,xx}(1 + \Sigma_{13}\sigma_{13})\delta_{13} = 0 \text{ at } x = x_c. \tag{3.4}$$

Our efforts to directly impose the continuity of velocity for fluid 1 at $x = x_c$ explicitly resulted in serious numerical difficulties, and so we took a different approach. The fluid mass of the substrate is conserved at all times, and so we used the following equation:

$$2\int_0^{x_c} h_{12}dx + 2\int_{x_c}^{x_\infty} h_{13}dx = V_1, \tag{3.5}$$

to compute $h_{13}(x_c, t)$; V_1 is the total dimensionless volume of fluid 1. To ensure this condition is sufficient and accurate, we evaluate the computed velocities at the contact line and verify that continuity of velocity is satisfied.

At the contact line, the force balance is always at equilibrium. In the general case, where surfactants are present, the balance between the interfacial forces at the contact point in dimensional form gives

$$\begin{aligned} \sigma^*_{13}\sin\theta^*_{13} + \sigma^*_{23}\sin\theta^*_{23} + \sigma^*_{12}\sin\theta^*_{12} &= 0, \\ \sigma^*_{13}\cos\theta^*_{13} + \sigma^*_{23}\cos\theta^*_{23} + \sigma^*_{12}\cos\theta^*_{12} &= 0. \end{aligned} \tag{3.6}$$

Combining the above equations, we get

$$\cos\theta^*_{int} = \frac{\sigma^{*2}_{13} - \sigma^{*2}_{23} - \sigma^{*2}_{12}}{2\sigma^*_{23}\sigma^*_{12}}, \quad \cos\theta^*_{ext} = \frac{\sigma^{*2}_{12} - \sigma^{*2}_{13} - \sigma^{*2}_{23}}{2\sigma^*_{23}\sigma^*_{13}}, \tag{3.7}$$

where $\theta^*_{int} = \theta^*_{12} - \theta^*_{23}$ and $\theta^*_{ext} = \theta^*_{23} - \theta^*_{13}$. Setting $\theta^*_{int} = \varepsilon\theta_a$, $\pi - \theta^*_{ext} = \varepsilon\phi_a$ and taking into consideration that $\cos(\varepsilon\theta) = 1 - \varepsilon^2\theta^2/2$, since $\varepsilon \ll 1$ in the lubrication limit, we derive the following relations in dimensionless form:

$$\theta_a^2 = \frac{-S[2\delta_{13}(1 + \Sigma_{13}\sigma_{13}) - S]}{\varepsilon^2(1 + \Sigma_{23}\sigma_{23})\delta_{12}(1 + \Sigma_{12}\sigma_{12})}, \tag{3.8}$$

$$\phi_a^2 = \frac{-S[2\delta_{12}(1 + \Sigma_{12}\sigma_{12}) + S]}{\varepsilon^2(1 + \Sigma_{23}\sigma_{23})\delta_{13}(1 + \Sigma_{13}\sigma_{13})}, \tag{3.9}$$

where S denotes the dimensionless spreading parameter defined as

$$S = \delta_{13}(1 + \Sigma_{13}\sigma_{13}) - \delta_{12}(1 + \Sigma_{12}\sigma_{12}) - (1 + \Sigma_{23}\sigma_{23}). \tag{3.10}$$

Using $\cos\theta^*_{int} = \underline{n}_{12} \cdot \underline{n}_{23}$ and $\cos\theta^*_{ext} = -\underline{n}_{23} \cdot \underline{n}_{13}$, we have $\theta_a = h_{12,x} - h_{23,x}$ and $\phi_a = h_{13,x} - h_{23,x}$. Thus, provided that the right hand sides of Eqs. (3.8) and (3.9) are positive and given that $h_{12,x} > h_{23,x}$, as well as $h_{13,x} > h_{23,x}$, we get

$$h_{12,x} = h_{23,x} + \sqrt{\frac{-S[2\delta_{13}(1 + \Sigma_{13}\sigma_{13}) - S]}{\varepsilon^2(1 + \Sigma_{23}\sigma_{23})\delta_{12}(1 + \Sigma_{12}\sigma_{12})}}, \tag{3.11}$$

$$h_{13,x} = h_{23,x} + \sqrt{\frac{-S[2\delta_{12}(1 + \Sigma_{12}\sigma_{12}) + S]}{\varepsilon^2(1 + \Sigma_{23}\sigma_{23})\delta_{13}(1 + \Sigma_{13}\sigma_{13})}}. \tag{3.12}$$

When $S > 0$ or the RHS of Eq. (3.8) or (3.9) becomes negative, we simply assume that $h_{12,x} = h_{23,x}$ or $h_{13,x} = h_{23,x}$, respectively. In the limit of $S = -\varepsilon^2$, and for surfactant-free fluids, Eqs. (3.11) and (3.12) reduce to the equations presented by Kriegsmann and Miksis.[10]

The contact line is a moving boundary, and therefore, additional information is needed in to order to determine its spatio-temporal evolution. To this end, we use the fact that the fluid volume of the drop must be conserved at all times. Therefore, the following relation:

$$2\int_0^{x_c} (h_{23} - h_{12})dx = V_2, \tag{3.13}$$

is used to compute the position of the contact line, x_c, at every time instant; V_2 is the dimensionless drop volume and it is equal to 1.

Regarding the boundary conditions for c_2 and m_2 at the contact line, we have to keep in mind that both c_2 and m_2 are volume concentrations, while the volume of the fluid at $x = x_c$ reduces to a line making them both singular. Fortunately, there is no need to find such a boundary condition for these variables since the corresponding terms in Eqs. (C10) and (C11) are multiplied by $h_{23} - h_{12}$ which is zero-valued at $x = x_c$ according to Eq. (3.3).

As mentioned earlier, our model permits the transfer of surfactant monomers from interfaces 12 and 23 to interface 13 and, conversely, directly through the contact line. The associated fluxes are given by

$$\left[u_{s,23}c_{23} - \frac{c_{23,x}}{Pe_{23}}\right]_{x=x_c} = \frac{dx_c}{dt}c_{23}|_{x=x_c} - \beta_{c12c23}J_{c12c23} - \beta_{c13c23}J_{c13c23}, \tag{3.14}$$

$$\left[u_{s,12}c_{12} - \frac{c_{12,x}}{Pe_{12}}\right]_{x=x_c} = \frac{dx_c}{dt}c_{12}|_{x=x_c} - \beta_{c13c12}J_{c13c12} - J_{c12c23}, \tag{3.15}$$

Downloaded 22 Dec 2011 to 129.31.211.195. Redistribution subject to AIP license or copyright; see http://pof.aip.org/about/rights_and_permissions

$$\left[u_{s,13}c_{13} - \frac{c_{13,x}}{Pe_{13}}\right]_{x=x_c} = \frac{dx_c}{dt}c_{13}|_{x=x_c} - J_{c13c12} - J_{c13c23}. \tag{3.16}$$

We should note that, at the contact line ($x = x_c$), the interfacial velocity, $u_{s,j}$, which appears in the LHS of Eqs. (3.14)–(3.16), is equal to the contact line velocity, dx_c/dt.

C. Initial conditions

The initial condition used for the film thickness, the position of the contact line, and the surfactant concentrations are given by

$$h_{23}(x, t=0) = h_{12}(x, t=0) + \frac{3V_2}{4}\left(1 - x^2\right), \tag{3.17}$$

$$h_{12}(x, t=0) = h_{13}(x, t=0) = \frac{V_1}{2x_\infty}, \tag{3.18}$$

$$x_c(t=0) = 1, \tag{3.19}$$

$$(c_{23}, c_{12}, c_{13}, c_2, m_2)(x, t=0) = (0, 0, 0, c_o, m_o). \tag{3.20}$$

We assume that at $t = 0$ the surfactant concentrations are in local equilibrium, and hence, the flux $J_2 = 0$. Thus, we have

$$c_o = m_o^{1/N}. \tag{3.21}$$

Substitution of Eq. (3.20) into Eq. (2.39) yields

$$\frac{1}{2}\left(m_o^{1/N} + m_o\right) = M, \tag{3.22}$$

which is solved numerically for a prescribed value of M. If $M < 1$, then the surfactant concentration is below the critical micelle concentration, and consequently, no micelles are present. In that case, we set $m_o = 0$ and $c_o = 2M$.

The resulting set of discrete equations is integrated in time using the implicit Euler method. An automatically adjusted time step is used for that purpose, which ensures convergence and optimizes code performance. The initial time step for all the simulations was $\Delta t = 10^{-6}$. The final set of algebraic equations is nonlinear, and they are solved at each time step using the Newton-Raphson method. The iterations of the Newton-Raphson method are terminated using 10^{-7} as a tolerance for the absolute error of the residual vector. The code was written in Fortran 90 and was run on a PC with Intel Core2 Duo E8400 at 3 GHz. Each run typically required 6–15 h to complete.

IV. RESULTS AND DISCUSSION

The spreading of a surfactant-laden liquid drop on a liquid substrate is a parametrically rich problem. Numerical solutions were obtained over a wide range of parameter values. For brevity, we choose a representative "base" case that has values of $\varepsilon^2 = 0.005$, $x_\infty = 10$, $V_1 = 20$, $\mu = 1$, $\rho = 1$, $\Sigma_{12} = \Sigma_{23} = \Sigma_{13} = 0.1$, $\delta_{12} = 1$, $\delta_{13} = 1.9$, $M = 8$, $Bo = 0.1$, $k_{c2c12} = k_{c2c23} = 1$, $R_{c2c12} = R_{c2c23} = 10$, $\beta_{c2c12} = \beta_{c2c23} = \beta_{c2c13} = 2$, $k_{c12c23} = k_{c13c12} = k_{c13c23} = k_{ev23} = k_{ev13} = 0$, $k_b = 1$, $N = 10$, $Pe_{12} = Pe_{23} = Pe_{13} = 10^3$, and $Pe_{c2} = Pe_{m2} = 10$. This set of parameters corresponds to the spreading of slender drops in the presence of a soluble surfactant, with concentration well above the critical micelle concentration, which can exist as a monomer at all the interfaces as well as micellar aggregates in the bulk drop. The surfactant is considered to be insoluble in the liquid substrate. The values chosen are reasonable, given the current knowledge of surfactant rate constants and the experiments, and demonstrate the main qualitative flow features that the model is capable of capturing.

A. Clean fluids

To set the stage for the discussion that follows, we begin by examining the spreading of a drop on a liquid substrate without any surfactants present ($M = 0$). In Fig. 2(a), we plot the time evolution of the contact line position for various values of the spreading parameter, S. To get this plot, we vary S by keeping constant $\delta_{12} = 1$ and changing the value of δ_{13} (i.e., $\delta_{13} = 1.9, 1.99, 1.995, 1.999, 2.1$). The rest of the parameters remain unchanged and the same as in the "base" case. As anticipated, we find that when the spreading parameter is negative the evolution of our system eventually leads to the formation of a stable lens-shaped drop (see Fig. 2(b) for the corresponding long time shapes at $t=10^4$). The initial extent of spreading cannot be maintained for $S = -0.11$, and the droplet retracts until it reaches equilibrium. Upon increasing the value of S, the drop equilibrates to larger aspect ratios. As shown in the figure, for $S = -0.0011$, the drop initially spreads followed by a short period of retraction. When the spreading parameter becomes positive ($S = 0.11$), there is sufficient force to drive complete spreading of the drop on the surface of the substrate; see Fig. 2(c) for the spatio-temporal evolution of the drop. The droplet radius grows with a power law exponent of order $t^{1/7}$ (see Fig. 2(a)) in agreement with theoretical predictions reported in the literature.[8,9] Further increase of the spreading parameter (not shown here) does not have any effect on the spreading exponent.

B. Surfactant-laden droplets

1. "Base" case

We next investigate the dynamics of a surfactant-laden droplet. The time evolution of the drop and the surfactant concentrations for the "base" case are shown in Figs. 3 and 4, respectively.

As already mentioned in Sec. III C, we assume that, initially, there is no surfactant present along the interfaces. The surfactant at $t = 0$ exists only in the bulk of the lens and in the form of monomers and micelles. At the early stages of the simulation, the lens retracts as it would normally do, for the given set of parameters, if there were no surfactant present. However, as time increases, the surfactant adsorbs at both interfaces of the lens resulting in the decrease of their surface tension; the profiles of c_{12} and c_{23} are shown in Figs. 4(a) and 4(b), respectively. This leads to the increase of the spreading parameter, evaluated at the contact line, and in turn to the deceleration of the retraction process until at some point ($t = 0.126$ for this set of parameter values), the drop starts spreading (see also Fig. 5(a) below). During the

Downloaded 22 Dec 2011 to 129.31.211.195. Redistribution subject to AIP license or copyright; see http://pof.aip.org/about/rights_and_permissions

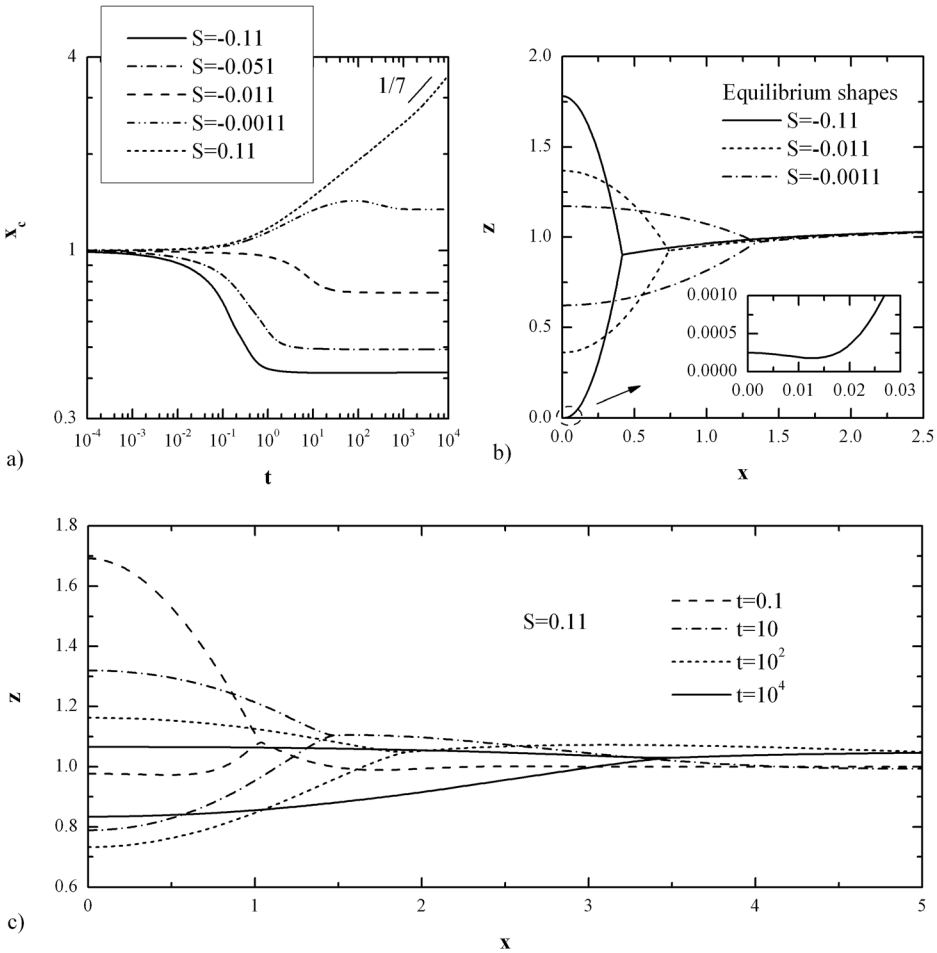

FIG. 2. (a) Time evolution of the contact line position for various values of the spreading parameter, S, (b) long time shapes of the lens (at $t = 10^4$) for negative S, and (c) spatio-temporal evolution of the lens for $S = 0.11$. We vary the value of S by changing the value of δ_{13} (1.9, 1.95, 1.99, 1.999, 2.1) while keeping $\delta_{12} = 1$.

retraction process, advection transfers surfactant towards the plane of symmetry giving rise to Marangoni stresses in the contact line region which oppose the lens retraction. Later on, when the lens starts spreading, the Marangoni stresses that are still present draw fluid from the substrate away from the lens; this results in the lifting of the contact line region and the creation of a ridge there (see Fig. 3(a)). As time increases, more surfactant monomers adsorb at the interfaces and, as a result, the corresponding bulk concentration, c_2, decreases (see Fig. 4(c)). This, in turn, leads the micelles to disassociate into monomers and the micelle concentration decreases very rapidly. Note that the corresponding figure (see Fig. 4(d)) is presented only for early times ($t \leq 10$) since after that point the concentration of micelles is very small. The dilation of the lens-air and lens-substrate interfaces, due to the spreading of the drop, causes continuous decrease of the corresponding surfactant concentrations and, consequently, to gradual deceleration of spreading. As the lens decelerates, diffusion damps the concentration gradients reducing Marangoni stresses leveling the lens until it eventually reaches equilibrium.

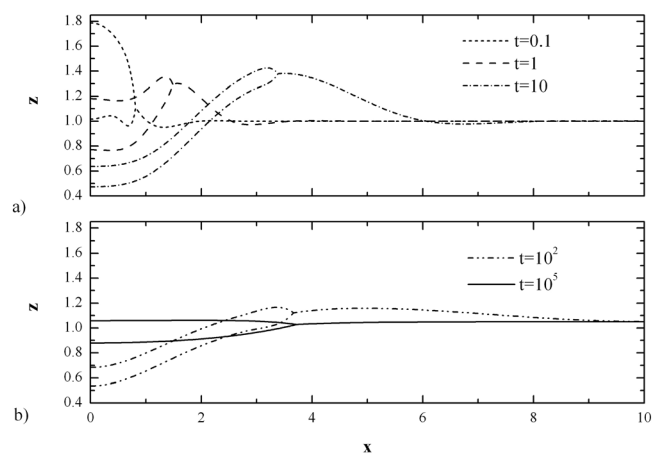

FIG. 3. Spatio-temporal evolution of the lens for the "base case." These parameters are kept unchanged in the subsequent figures unless noted otherwise.

2. Effect of surfactant mass, M

Next, we examine the effect of the mass of surfactant emplaced in the drop by varying the parameter M. As shown in Fig. 5(c), during the early stages of the simulation, the surfactant adsorbs rapidly at both interfaces and the corresponding concentrations increase following a power law almost equal to t, regardless of the value of M; the time evolution of $c_{12}(0,t)$ is very similar to $c_{23}(0,t)$ and is not presented here. When the initial amount of surfactant is large, the monomers in the bulk are replenished by the disassociation of micelles, which act as a large reservoir releasing surfactant monomers and maintaining rapid spreading for longer times (see Figs. 5(d) and 5(e)). On the other hand, for small values of M, the monomers and the micelles in the bulk become depleted

Downloaded 22 Dec 2011 to 129.31.211.195. Redistribution subject to AIP license or copyright; see http://pof.aip.org/about/rights_and_permissions

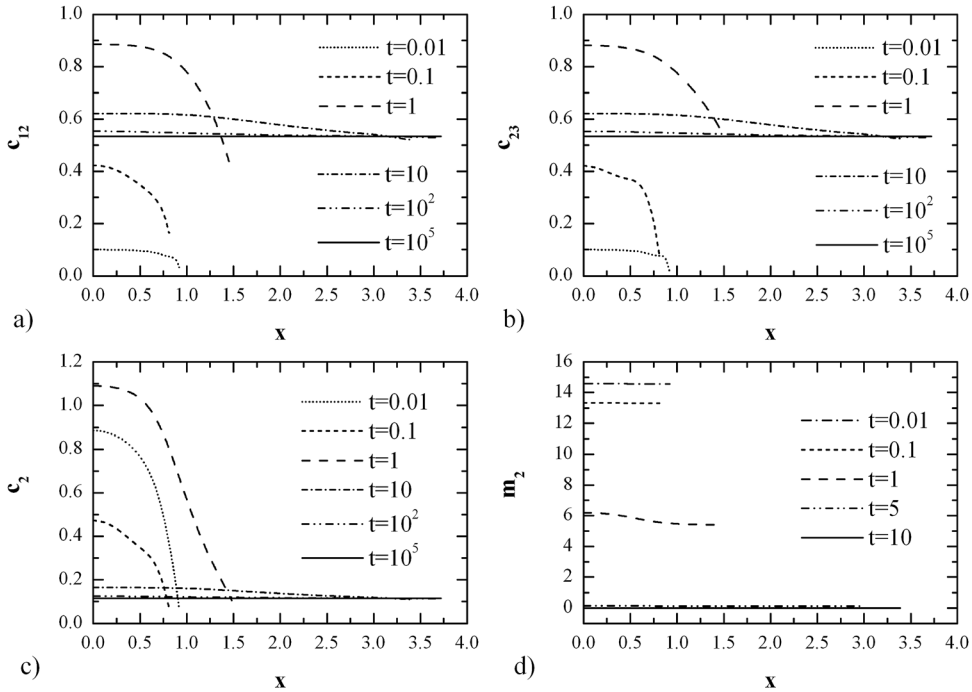

FIG. 4. Spatio-temporal evolution of the surfactant concentrations for the "base case."

soon leading to a smaller extent of spreading. We can see in Fig. 5(a) that the final extent of spreading depends monotonically on the amount of surfactant, in agreement with previous experimental findings;[19] the drop profiles close to equilibrium ($t = 10^5$) for four different values of M can be seen in Fig. 6.

Regarding the spreading rates, increasing the available amount of surfactant results in the increase of the spreading exponent, for moderate values of M. However, for large values of M, the front advances with a power law almost equal to $t^{1/2}$, a rate greatly in excess of the $t^{1/7}$ predicted for the case of clean fluids. Interestingly, these spreading rates are

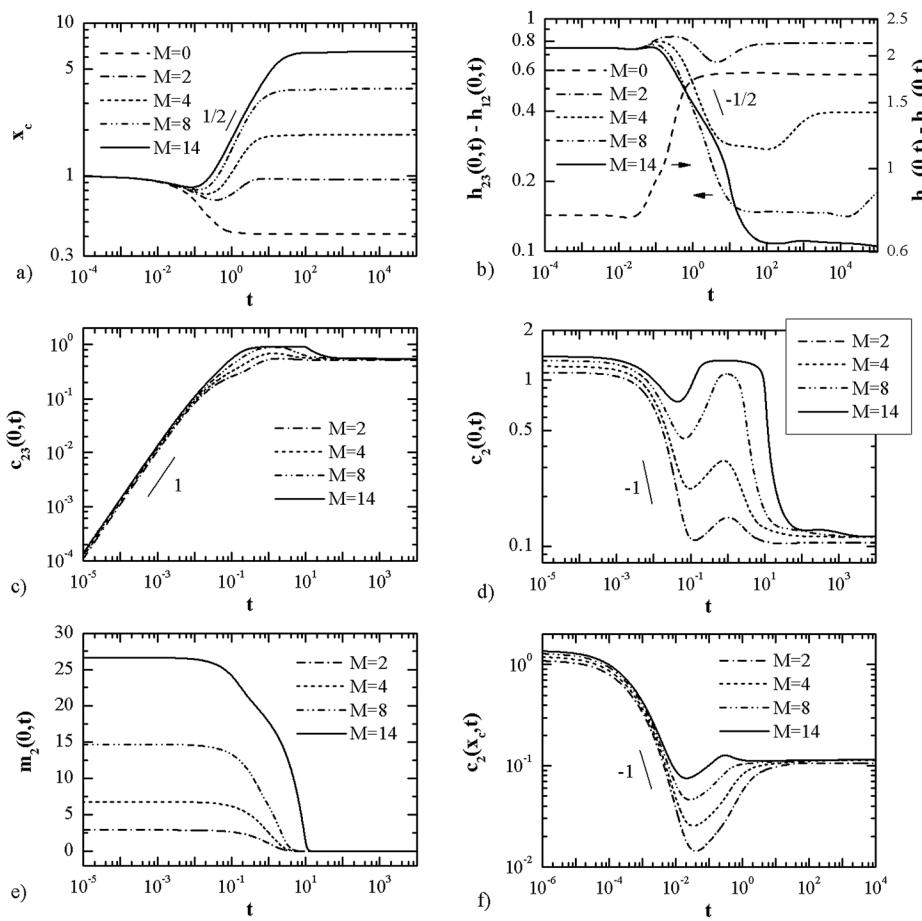

FIG. 5. Time evolution of the (a) position of the contact line, x_c, and (b) thickness of the lens at $x = 0$, (c) $c_{23}(0,t)$, (d) $c_2(0,t)$, (e) $m_2(0,t)$, (f) $c_2(x_c,t)$ for different values of the surfactant mass, M.

Downloaded 22 Dec 2011 to 129.31.211.195. Redistribution subject to AIP license or copyright; see http://pof.aip.org/about/rights_and_permissions

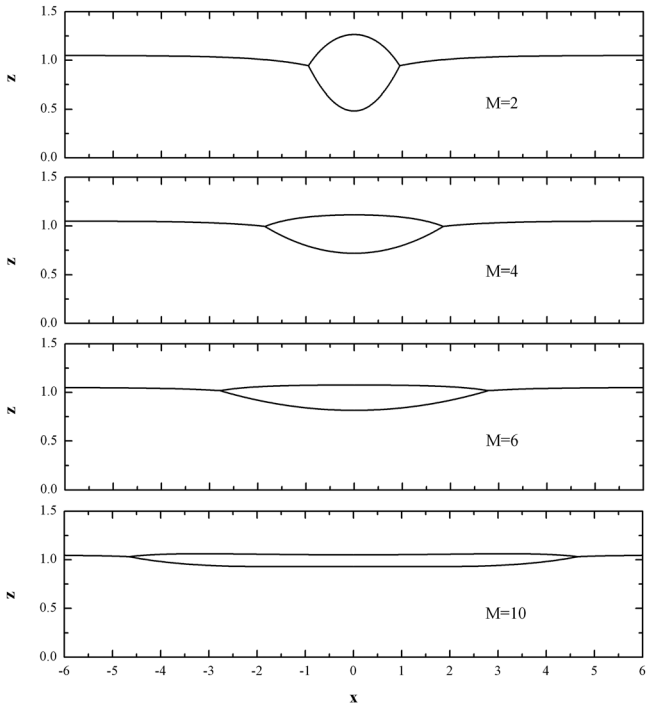

FIG. 6. Long-time lens shapes at $t = 10^5$ for different values of the surfactant mass, M.

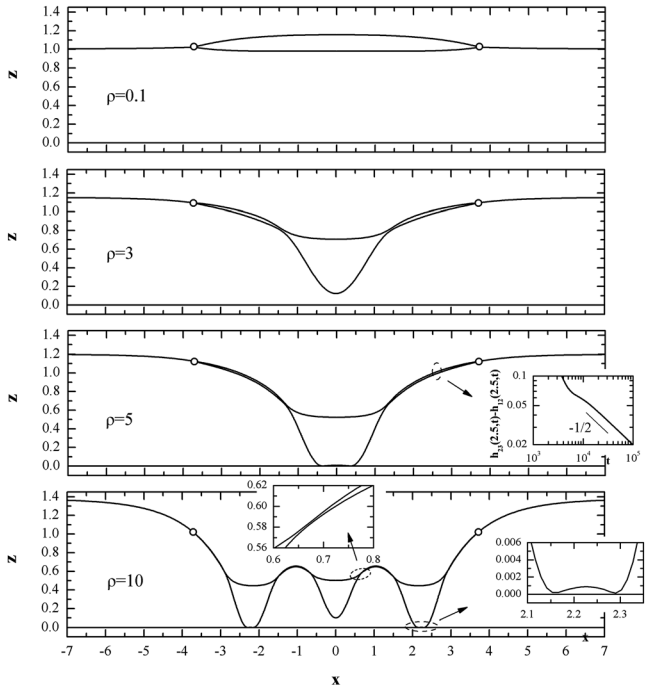

FIG. 7. Long-time drop shapes at $t = 10^5$ for different density ratios, ρ. The open circle symbol denotes the position of the contact line. The inset for $\rho = 5$ shows that the layer at $x = 2.5$ thins following a power law of approximately $t^{-1/2}$.

very close to those reported by several experimentalists for the spreading of surfactant-laden drops on organic substrate layers.[16,21,22] At this point, however, it should be noted that our model refers to a planar drop, and therefore, a direct comparison with experimental values is not possible. Nevertheless, it is evident that the computed power law exponents are in qualitative agreement with experiments showing the significant increase of the spreading rate due to the presence of surfactants. In addition, as the drop spreads out, its thickness at $x = 0$ decreases almost with $t^{-1/2}$ (see Fig. 5(b)). In this figure, we also observe that for large values of M the drop thickness still changes significantly by the end of the simulation ($t = 10^5$), in contrast with the contact line position which is unaffected, indicating that more time is needed for our system to reach its final equilibrium state.

3. Effect of the density and viscosity ratios and substrate depth

The effect of density ratio, ρ, is explored in Fig. 7, where we plot the equilibrium shapes for $\rho = 0.1$, 3, 5, and 10. As expected, when the drop is lighter than the bottom fluid ($\rho = 0.1$), the lens rests on top of the substrate, whereas for $\rho > 1$, the drop sinks and may even touch the solid wall. An interesting feature is that, in all cases presented in this figure, the contact line (shown by the open circle) remains approximately at the same position. For $\rho = 3$ and 5, the drop spreads due to the presence of the surfactant but collapses under its own weight, towards the plane of symmetry, leaving a very thin layer of fluid along the liquid substrate. The inset for $\rho = 5$ presents the evolution of the layer thickness at $x = 2.5$ in log-log scale and as we can see the layer thins following a power law of approximately $t^{-1/2}$. As we can see in the figure, the situation becomes a bit more complicated for heavier droplets. For $\rho = 10$, the droplet splits into three parts which are connected by a thin layer of fluid. As we have already seen in Figs. 2 and 3, Marangoni stresses draw part of the liquid below the drop towards the contact line region raising this part of the drop. Obviously, there is interplay between gravitational and Marangoni forces which can give rise to this kind of phenomenon for heavy drops.

The effect of varying the viscosity ratio, μ, on the dynamics of the drop is examined in Fig. 8(a) where we plot the position of the contact line and the drop thickness at $x = 0$ for $\mu = 0.1$, 1, and 100. We expect that the viscosity ratio would affect the flow time scales. Indeed, the enhanced mobility of the drop for low values of the viscosity ratio results in faster retraction during the early stages of the simulation and allows for the system to reach equilibrium sooner. Although the spreading rate is not affected significantly, we see that during the late stages of the simulation, the system needs considerably more time to reach its final state for large values of μ.

Another important parameter of our model is the initial depth of the substrate, and its effect is examined in Fig. 8(b). As expected, increasing the initial height, the drop feels less the presence of the solid substrate resulting in higher spreading rates due to the decreased resistance to the flow. It is important to note, however, that this parameter cannot be increased indefinitely without invalidating the lubrication approximation underlying the present model.

4. Spreading and recoiling

In Secs. IV B 1–IV B 3, surfactant is present only in the bulk drop along the lens-substrate and lens-air interfaces. The dynamics when the surfactant is allowed to diffuse away

Downloaded 22 Dec 2011 to 129.31.211.195. Redistribution subject to AIP license or copyright; see http://pof.aip.org/about/rights_and_permissions

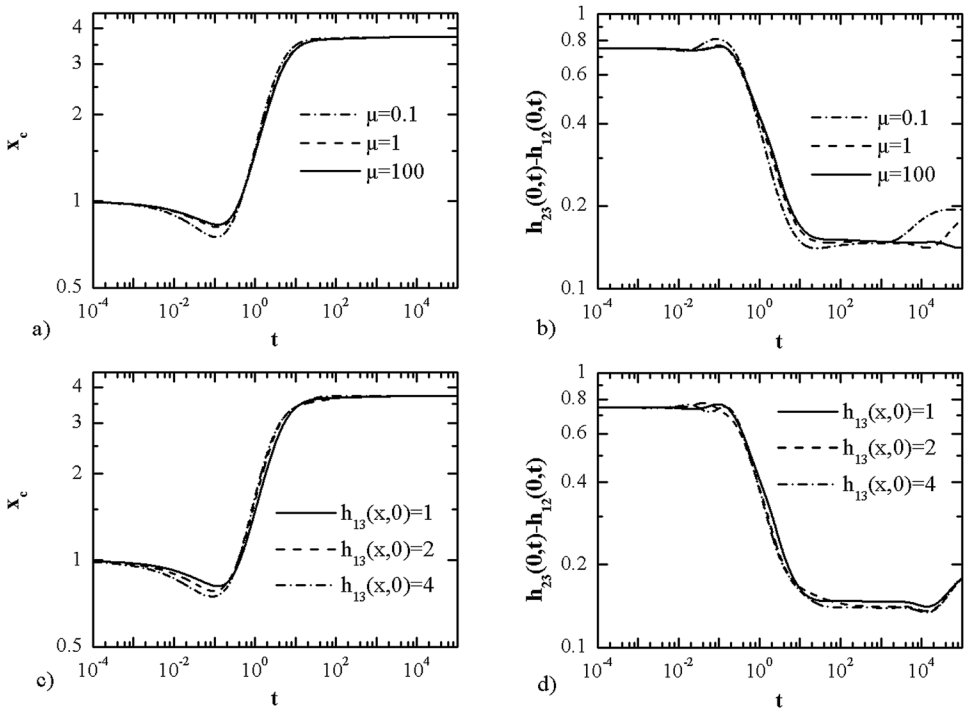

FIG. 8. Time evolution of x_c and $h_{23}(0,t) - h_{12}(0,t)$ for (a) different viscosity ratios μ and (b) different initial heights of the liquid substrate.

from the drop along the substrate-air interface is of considerable interest in terms of real surfactant behaviour. As already mentioned in Sec. II, our model allows the transport of surfactant from one interface to another through the contact line using the boundary conditions shown in Eqs. (3.14)–(3.16) where the corresponding fluxes are given by Eqs. (B9)–(B11). Figures 9 and 10 present a series of simulations for various values of k_{c13c12} while keeping $k_{c13c23} = k_{c12c23} = 0$. These simulations refer to cases where the surfactant monomers that have been adsorbed at the lens-substrate interface can adsorb through the contact line at the substrate-air interface and diffuse away from the drop.

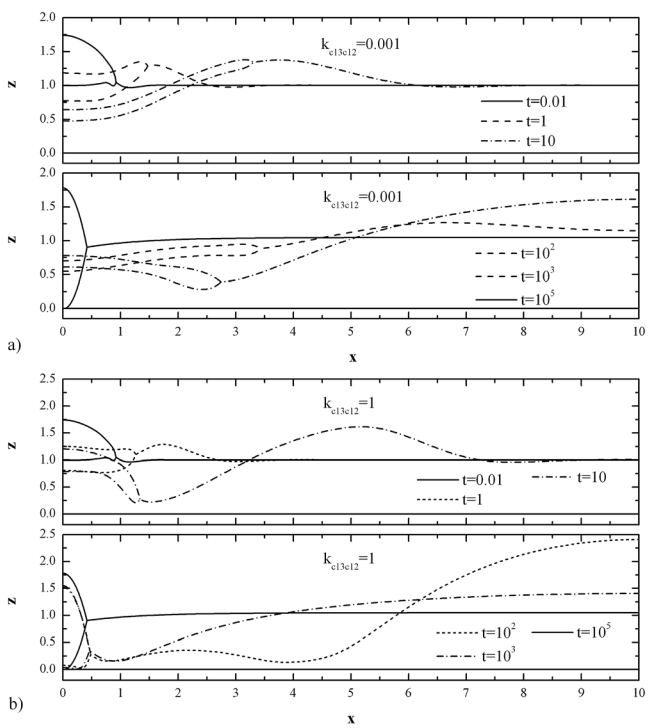

FIG. 9. Time evolution of the lens for (a) $k_{c13c12} = 0.001$ and (b) $k_{c13c12} = 1$.

During the early stages of the simulations, the surfactant in the bulk drop adsorbs at the lens-substrate and lens-air interfaces initiating the spreading process. As time increases, more surfactant adsorbs at the substrate-air interface through the contact line resulting in an increase in c_{13}. This leads to the decrease of the substrate-air surface tension and, in turn, in the deceleration of the spreading process. Eventually, the drop starts to retract until it reaches equilibrium. We should note here that this simulation presents some interesting similarities with the experiments presented by van Nierop *et al.*,[14] where they have observed droplets of oil containing oleic acid to spread and then recoil on an aqueous solution of sodium hydroxide. Oleic acid and NaOH react at the interface producing sodium oleate which acts as a surfactant at the oil-water interface. These authors have suggested that the recoiling was due to the diffusion of the surfactant away from the oil-water interface. Although our model does not formally include a model for the interfacial reaction of two reagents producing surfactant, the kinetics of the adsorption process at the lens-substrate interface will play a similar role to the kinetics of the interfacial reaction.

For small values of the kinetic parameter, k_{c13c12}, the surfactant is released slowly to the substrate-air interface and the spreading process resembles the case where no surfactant is present away from the drop (see Figs. 3(a) and 9(a)). Obviously, as shown in Fig. 9(b), this is not the case when k_{c13c12} becomes large. In this case, the surfactant adsorbs faster at the substrate-air interface which results in the accumulation of surfactant in the contact line region (see Fig. 10(b)). This gives rise to strong Marangoni stresses which affect significantly the shape of the substrate-air interface. The bottom

Downloaded 22 Dec 2011 to 129.31.211.195. Redistribution subject to AIP license or copyright; see http://pof.aip.org/about/rights_and_permissions

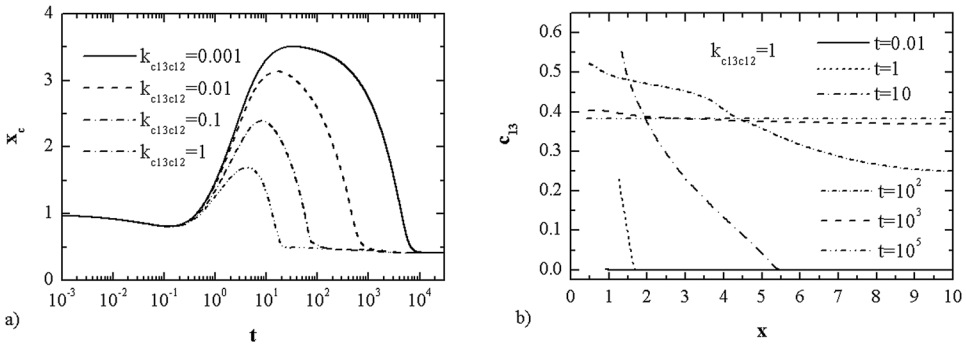

FIG. 10. (a) Effect of k_{c13c12} on the contact line position. (b) Time evolution of the substrate-air monomer concentration, c_{13} for $k_{c13c12} = 1$.

fluid is drawn away from that region, and the height of the contact line decreases while the rest of the drop sits higher. As time passes, the surfactant diffuses away from the drop weakening the Marangoni stresses along the substrate-air interface, and as a result, the fluid flows back towards the plane of symmetry. It is worth noting that Fraaije and Cazabat[9] reported a similar phenomenon when they placed an oil drop on a thin layer of glycerol/water mixture. The substrate in the neighborhood of the drop retracted leaving the oil drop on the petri dish bottom, and after several seconds, the substrate flowed back to the drop lifting it. Fraaije and Cazabat suggested that an explanation for this phenomenon could be that the droplet is initially so large that pierces the substrate. They have also suggested that this could be due to inertial effects on the substrate liquid as it is drawn by the rapidly spreading oil and until countercurrent is set up in the substrate. We cannot help but wonder whether the described phenomenon could also be due to the presence of contaminants giving rise to Marangoni stresses at the substrate-air interface as shown in Fig. 9(b).

Another mechanism through which a drop could initially spread and then recoil is when the surfactant is volatile (see Fig. 11). In this case, the interfacial surfactant concentration increases until at some point it reaches a maximum and then starts to decrease due to the dilation of the interfaces, as the drop spreads out, and the "evaporation." Despite the decrease of the concentration, the drop continues to spread a bit longer until the spreading parameter decreases to such value that the extent of spreading cannot be maintained. At that point, the drop starts to retract and the surfactant concentration remains almost steady for some time since the "evaporation" of surfactant is compensated by the contraction of the interfaces. Eventually, the drop decelerates as it reaches equilibrium and the surfactant gets depleted.

5. Self sustained oscillations

As already mentioned, recent experiments, performed by Stocker and Bush,[24] on spontaneously oscillating surfactant-laden oil drops revealed some very interesting features, shedding light on the underlying mechanism. They have shown that the retraction of the drop is initiated by the rapid formation of thin films at the lens leading edge due to growth of perturbations in the azimuthal direction, releasing surfactant at the water-air interface and decreasing its surface tension. The ejection process is, indeed, complex and modeling it in detail is beyond the scope of this paper. However, given the versatility of the model, it is interesting to see if it predicts this oscillatory behavior using an *ad hoc* approach to model these eruption events.

Let us assume that, during the early stages of the spreading, surfactant is present only in the bulk lens along the lens-air and lens-substrate interfaces. As the lens spreads, the contact angle decreases. We assume that when the contact angle decreases below a certain limit, $\theta_{a,l}$, the leading edge becomes unstable, erupting and releasing surfactant at the substrate-air interface. The release is modeled by allowing surfactant to diffuse away from the lens using a finite value for k_{c13c12} as we have already done in Fig. 9. At that point, the lens begins to retract due to the decrease of the substrate-air surface tension, and as a result, the contact angle increases. We assume that when the contact angle increases beyond a certain limit, $\theta_{a,u}$, the leading edge becomes stable and the release of surfactant stops. For our simulations,

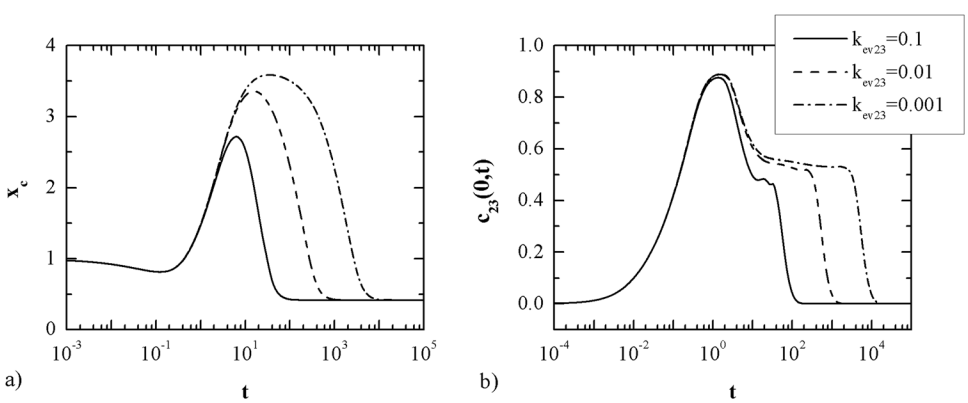

FIG. 11. Time evolution of (a) the position of the contact line x_c and (b) $c_{23}(0,t)$ for various "evaporation" rates.

Downloaded 22 Dec 2011 to 129.31.211.195. Redistribution subject to AIP license or copyright; see http://pof.aip.org/about/rights_and_permissions

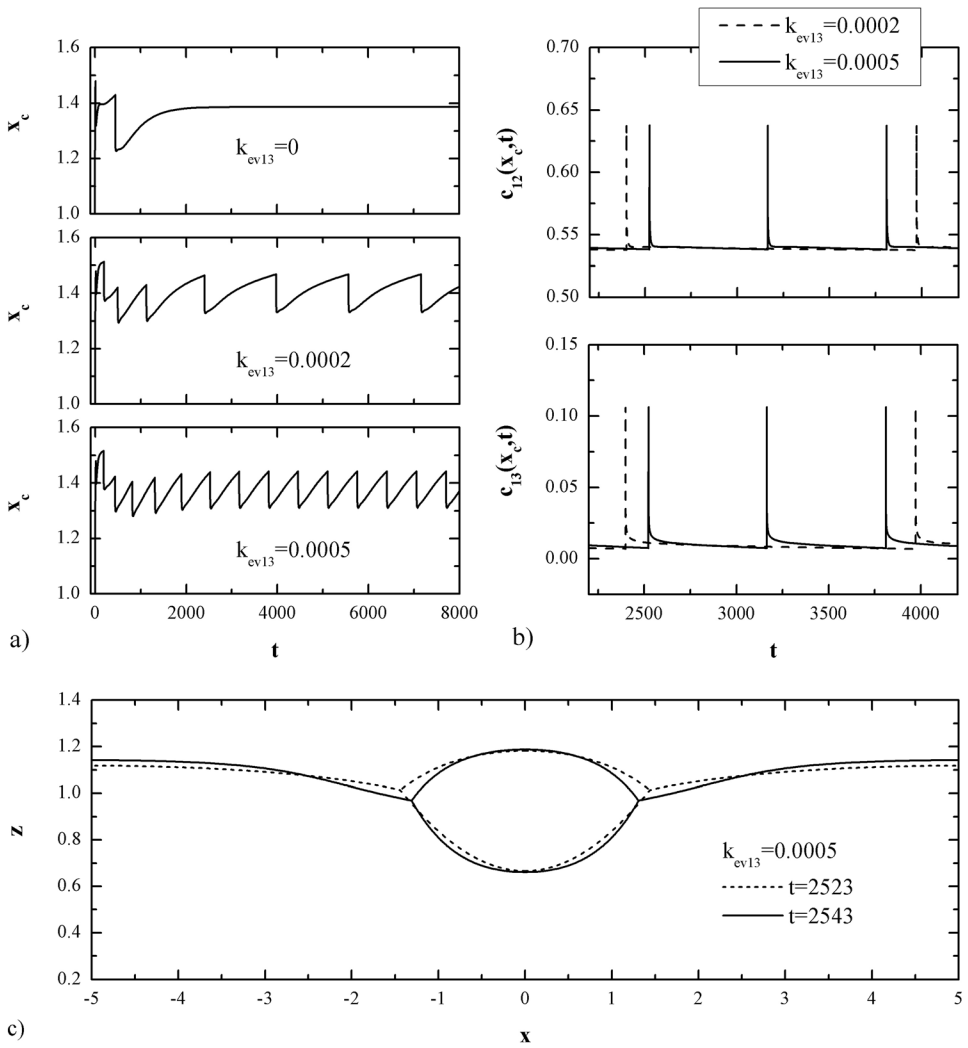

FIG. 12. (a) Effect of the evaporation rate on the contact line position, x_c. Time evolution of (b) $c_{12}(x_c,t)$ and $c_{23}(x_c,t)$ for two different evaporation rates. (c) Lens profiles at $t = 2523$ and $t = 2543$ for $k_{ev13} = 0.0005$.

shown in Fig. 12, we have used $\theta_{a,l} = 0.75$, $\theta_{a,u} = 1.25$ for which the given value of ε correspond to the contact angles of 3° and 5°, respectively. We should also note that for this simulation we have considered that the interfacial surfactant and the monomer in the bulk are initially at equilibrium and that $\beta_{c2c13} = 0.1$.

First, we examine the case where "evaporation" is not present. Stocker and Bush reported that when they placed a lid on the petri dish, the oscillations stopped. Indeed, we find that when there is no "evaporation" ($k_{ev13} = 0$), the lens reaches equilibrium after just two "ejection" events that take place early (see Fig. 12(a)). During the initial spreading of the drop, the contact angle decreases until at some point becomes lower than $\theta_{a,l}$ and surfactant is released to the substrate-air interface causing the retraction of the drop. The released surfactant diffuses away from the contact line region with time leading to the reinitiation of our system. After a couple of "ejection" events and since we consider only a finite amount of liquid substrate, the surfactant concentration at the substrate-air interface becomes such that the contact angle remains always higher than $\theta_{a,l}$; after that point, no "ejection" takes place and the system reaches equilibrium. It is expected that the exact number of these "ejection" events may vary slightly, depending on factors like the selection of $\theta_{a,l}$,$\theta_{a,u}$, and the length of our domain (here we use $x_\infty = 5$) and the solubility of surfactant to the substrate-air interface.

The situation becomes quite different when we allow for the surfactant that has diffused along the substrate-air interface to "evaporate." In this case, we find that the lens oscillates for very long times in broad agreement with observations; the shape of the lens at two time instants, where the contact line is at its maximum and minimum positions, is shown in Fig. 12(d). We can see in Fig. 12(a) that increasing the "evaporation" rate, by increasing the value of k_{ev13}, results in the decrease of the time period of the oscillations. This should be expected since in this case less time is needed in order for the surfactant to "evaporate" and thus for the contact line to reach its maximum position, before a new "ejection" event takes place. This is also shown clearly in Fig. 12(c) where we present time evolution of the substrate-air surfactant concentration at the contact line. When the "ejection" starts $c_{13}(x_c,t)$ suddenly increases and then its concentration decreases due to the "evaporation." The reason for the sudden increase of $c_{12}(x_c,t)$, shown in Fig. 12(d), is quite different since it is due to the contraction of the lens-substrate interface as the lens starts to retract. As time increases, the total amount of surfactant present in the

Downloaded 22 Dec 2011 to 129.31.211.195. Redistribution subject to AIP license or copyright; see http://pof.aip.org/about/rights_and_permissions

system will decrease resulting in higher contact angles until at some point "ejection" events stop, and the lens reaches a new equilibrium.

V. CONCLUDING REMARKS

We examine the spreading of surfactant-laden lenses over liquid substrates for surfactants with concentrations beyond the critical micelle concentration. Lubrication theory and rapid vertical diffusion of the surfactant in the bulk are used to derive a coupled system of evolution equations for the interface positions, surfactant monomer interfacial and bulk concentrations, and micelle bulk concentration. The model accounts for Marangoni-driven spreading, interfacial and bulk diffusion, sorption kinetics, "evaporation" of volatile surfactants, the formation and breakup of micelles in the bulk, and for surfactant adsorption at the solid substrate. Moreover, this model takes into account the effect of local surfactant concentration on contact line motion and the possibility of surfactant adsorption directly through the contact line. The model incorporates the essential physics and surface chemistry of the problem, coupled together with the hydrodynamics, and is sufficiently complex to capture and explain realistic phenomena. This model is solved numerically using the finite-element method and the results of an extensive parametric analysis are presented.

Our numerical results have shown that the final extent of spreading depends monotonically on the mass of the surfactant deposited and that, for fairly large amounts of surfactant, the leading edge advances following a power-law dependence of $t^{1/2}$. Eventually, the leading edge stops advancing, while significantly more time may be needed before the lens acquires its final equilibrium shape, depending on parameters like the viscosity ratio and the total amount of surfactant present. The spreading is accompanied in several cases by the formation of a ridge in the contact line region because of the presence of Marangoni stresses. These findings are in agreement with previous observations of experiments in the literature. We have also studied cases where the lens may initially spread and then recoil as surfactant is removed from the lens either due to the diffusion of surfactant along the substrate-air interface or "evaporation." In the former case and in the presence of high Marangoni stresses, it is possible for the liquid substrate to retract away from the lens leaving it on the solid surface only to return later and lift the lens from the bottom. Finally, we used our model to examine the mechanism that was proposed by Stocker and Bush[24] for the spontaneous oscillations of oil lenses and found that, indeed when surfactant is released via rapid ejections onto the substrate-air interface and is allowed to "evaporate," it is possible for a lens to oscillate with a time period that depends on the "evaporation" rate.

ACKNOWLEDGMENTS

The authors would like to acknowledge the helpful contribution of David Beacham and the support of the Engineering and Physical Science Research Council through Grant Nos. EP/E056466 and EP/E046029/1.

APPENDIX A: SURFACTANT TRANSPORT FLUXES

This appendix contains expressions for the fluxes that determine how the surfactant transfers between the different phases, derived from kinetic laws for the "reactions" presented in Sec. II B,

$$J^*_{c2c23} = -D^*_{c2}\left[\underline{n}\cdot\nabla c^*_2\right]_{z^*=h^*} = k^*_1 c^*_2\big|_{z^*=h^*}\left(1-\frac{c^*_{23}}{c^*_{23,\infty}}\right) - k^*_2 c^*_{23}, \tag{A1}$$

$$J^*_{c2c12} = -D^*_{c2}\left[\underline{n}\cdot\nabla c^*_2\right]_{z^*=0} = k^*_3 c^*_2\big|_{z^*=0}\left(1-\frac{c^*_{12}}{c^*_{12,\infty}}\right) - k^*_4 c^*_{12}, \tag{A2}$$

$$J^*_2 = k^*_5 c^{*N}_2 - k^*_6 m^*_2, \tag{A3}$$

$$J^*_{c12c23} = \left[k^*_7 c^*_{12}\left(1-\frac{c^*_{23}}{c^*_{23,\infty}}\right) - k^*_8 c^*_{23}\left(1-\frac{c^*_{12}}{c^*_{12,\infty}}\right)\right]_{x^*=x^*_c}, \tag{A4}$$

$$J^*_{c13c12} = \left[k^*_9 c^*_{13}\left(1-\frac{c^*_{12}}{c^*_{12,\infty}}\right) - k^*_{10} c^*_{12}\left(1-\frac{c^*_{13}}{c^*_{13,\infty}}\right)\right]_{x^*=x^*_c}, \tag{A5}$$

$$J^*_{c13c23} = \left[k^*_{11} c^*_{13}\left(1-\frac{c^*_{23}}{c^*_{23,\infty}}\right) - k^*_{12} c^*_{23}\left(1-\frac{c^*_{13}}{c^*_{13,\infty}}\right)\right]_{x^*=x^*_c}, \tag{A6}$$

where x^*_c denotes the position of the contact line at time t^*. Here, $c^*_{j,\infty}(i = 13, 23, 12)$ represent the interfacial surfactant concentration at maximum packing. The non-linear terms in Eqs. (A1)–(A2) and (A4)–(A5) imply that when $c^*_j \to c^*_{j,\infty}$ $(j = 13, 23, 12)$, that is, when an interface becomes fully packed with monomers, no further surfactant is adsorbed. The non-linear term is obtained by taking into consideration the available space S_j $(j = 13, 23, 12)$ at the interface, indicating that there is limit to the amount of monomers that can adsorb at both surfaces. At equilibrium, this is the Langmuir adsorption isotherm. This set of laws allows the surfactant to move from monomer to micelle, from bulk to either surfaces, and also allows surfactant to transfer through the contact line.

APPENDIX B: SCALED ADVECTION-DIFFUSION EQUATIONS AND RELEVANT FLUXES

The height evolution equations are coupled to the scaled surfactant transport equations that become

$$c_{23,t} + \left(u_{s,23}c_{23}\right)_x = \frac{1}{Pe_{23}}c_{23,xx} + J_{c2c23} + J_{ev23}, \tag{B1}$$

$$c_{12,t} + \left(u_{s,12}c_{12}\right)_x = \frac{1}{Pe_{12}}c_{12,xx} + J_{c2c12}, \tag{B2}$$

$$c_{13,t} + \left(u_{s,13}c_{13}\right)_x = \frac{1}{Pe_{13}}c_{13,xx} + J_{ev13}, \tag{B3}$$

$$c_{2,t} + u_2 c_{2,x} + w_2 c_{2,x} = \frac{1}{Pe_{c2}}\left(c_{2,xx} + \frac{c_{2,zz}}{\varepsilon^2}\right) - J_2, \tag{B4}$$

Downloaded 22 Dec 2011 to 129.31.211.195. Redistribution subject to AIP license or copyright; see http://pof.aip.org/about/rights_and_permissions

$$m_{2,t} + u_2 m_{2,x} + w_2 m_{2,x} = \frac{1}{Pe_{m2}}\left(m_{2,xx} + \frac{m_{2,zz}}{\varepsilon^2}\right) + J_2. \quad \text{(B5)}$$

The dimensionless groups $Pe_i = U^* L^*/D_i^*$ $(i = 12, 23, 13, c2, m2)$ are Peclet numbers representing a ratio of convective to diffusive time scales for the monomers at the interfaces, and the monomers and the micelles in the bulk, respectively. The dimensionless fluxes J_i that appear in the above equations are expressed by

$$J_{c2c23} = k_{c2c23}\left(R_{c2c23} c_2|_{z=h_{23}}(1 - c_{23}) - c_{23}\right), \quad \text{(B6)}$$

$$J_{c2c12} = k_{c2c12}\left(R_{c2c12} c_2|_{z=h_{23}}(1 - c_{12}) - c_{12}\right), \quad \text{(B7)}$$

$$J_2 = k_b\left(c_2^N - m_2\right), \quad \text{(B8)}$$

$$J_{c12c23} = k_{c12c23}[R_{c12c23} c_{12}(1 - c_{23}) - c_{23}(1 - c_{12})]_{x=x_c}, \quad \text{(B9)}$$

$$J_{c13c12} = k_{c13c12}[R_{c13c12} c_{13}(1 - c_{12}) - c_{12}(1 - c_{13})]_{x=x_c}, \quad \text{(B10)}$$

$$J_{c13c23} = k_{c13c23}[R_{c13c23} c_{13}(1 - c_{23}) - c_{23}(1 - c_{13})]_{x=x_c}, \quad \text{(B11)}$$

$$J_{ev23} = -k_{ev23} c_{23}, \quad \text{(B12)}$$

$$J_{ev13} = -k_{ev13} c_{13}, \quad \text{(B13)}$$

where the dimensionless parameters k_i and R_i are given by

$$(k_{c2c23}, k_{c2c12}, k_b, k_{ev23}, k_{ev13}) = \frac{L^*}{U^*}\left(k_2^*, k_4^*, k_6^*, k_{13}^*, k_{14}^*\right), \quad \text{(B14)}$$

$$(k_{c12c23}, k_{c13c12}, k_{c13c23}) = \left(k_8^*, k_{10}^*, k_{12}^*\right)/U^*, \quad \text{(B15)}$$

$$(R_{c2c23}, R_{c2c12}, R_{c12c23}, R_{c13c12}, R_{c13c23}) = \left(\frac{k_1^* c_{cmc}^*}{k_2^* c_{23,\infty}^*}, \frac{k_3^* c_{cmc}^*}{k_4^* c_{12,\infty}^*}, \frac{k_7^* c_{12,\infty}^*}{k_8^* c_{23,\infty}^*}, \frac{k_9^* c_{13,\infty}^*}{k_{10}^* c_{12,\infty}^*}, \frac{k_{11}^* c_{13,\infty}^*}{k_{12}^* c_{23,\infty}^*}\right). \quad \text{(B16)}$$

The kinetic parameters k_i, from left to the right as they appear in Eq. (B14), control the sorption kinetics at the interfaces, the breakup and formation rate of micellar aggregates in the bulk, and the kinetics of interfacial surfactant "evaporation." The kinetic parameters in Eq. (2.15) control the sorption kinetics at the contact line. The parameter R_i is a measure of the affinity of the surfactant to the liquid-air interface and substrate. Small values of R_{c2c23} and R_{c2c12} signify the tendency of the surfactant to remain in the bulk in the form of micelles.[26,29] Similarly, when R_{c12c23} is small, the surfactant at the contact line has the tendency to remain at the lens-air interface instead of adsorbing at the substrate.

APPENDIX C: WEAK FORMULATION OF THE GOVERNING EQUATIONS

Applying the divergence theorem, the weak form of the equations for the position interfaces and the interfacial surfactant monomers (Eqs. (2.22) and (2.34)–(2.38)) become

$$\int_{x_c}^{x_\infty}\left(h_{13,t}\phi_i - \phi_{i_x}\int_0^{h_{13}} u_1 dz\right)dx + \left[\phi_i\int_0^{h_{13}} u_1 dz\right]_{x_c}^{x_\infty} = 0, \quad \text{(C1)}$$

$$\int_0^{x_c}\left(h_{13,xx}\phi_i + \phi_{i_x} h_{13,x}\right)dx - \left[\phi_i h_{13,x}\right]_0^{x_c} = 0, \quad \text{(C2)}$$

$$\int_0^{x_c}\left(h_{12,t}\phi_i - \phi_{i_x}\int_0^{h_{12}} u_1 dz\right)dx + \left[\phi_i\int_0^{h_{12}} u_1 dz\right]_0^{x_c} = 0, \quad \text{(C3)}$$

$$\int_0^{x_c}\left(h_{12,xx}\phi_i + \phi_{i_x} h_{12,x}\right)dx - \left[\phi_i h_{12,x}\right]_0^{x_c} = 0, \quad \text{(C4)}$$

$$\int_0^{x_c}\left(h_{23,t}\phi_i - \phi_{i_x}\int_0^{h_{12}} u_1 dz - \phi_{i_x}\int_{h_{12}}^{h_{23}} u_2 dz\right)dx + \left[\phi_i\left(\int_0^{h_{12}} u_1 dz + \int_{h_{12}}^{h_{23}} u_2 dz\right)\right]_0^{x_c} = 0, \quad \text{(C5)}$$

$$\int_0^{x_c}\left(h_{23,xx}\phi_i + \phi_{i_x} h_{23,x}\right)dx - \left[\phi_i h_{23,x}\right]_0^{x_c} = 0, \quad \text{(C6)}$$

$$\int_0^{x_c}\left[\left(c_{23,t} - J_{c2c23} - J_{ev23}\right)\phi_i - \left(u_{s,23} c_{23} - \frac{c_{23,x}}{Pe_{23}}\right)\phi_i x\right]dx + \left[u_{s,23} c_{23} - \frac{c_{23,x}}{Pe_{23}}\right]_0^{x_c} = 0, \quad \text{(C7)}$$

$$\int_0^{x_c}\left[\left(c_{12,t} - J_{c2c12}\right)\phi_i - \left(u_{s,12} c_{12} - \frac{c_{12,x}}{Pe_{12}}\right)\phi_i x\right]dx + \left[u_{s,12} c_{12} - \frac{c_{12,x}}{Pe_{12}}\right]_0^{x_c} = 0, \quad \text{(C8)}$$

$$\int_{x_c}^{x_\infty}\left[\left(c_{13,t} - J_{ev13}\right)\phi_i - \left(u_{s,13} c_{13} - \frac{c_{13,x}}{Pe_{13}}\right)\phi_i x\right]dx + \left[u_{s,13} c_{13} - \frac{c_{13,x}}{Pe_{13}}\right]_{x_c}^{x_\infty} = 0. \quad \text{(C9)}$$

Note that each fourth order partial differential equation has been decomposed into two second order differential equations. The presence of $h_{23} - h_{12}$ in the denominator of several terms in Eqs. (2.37) and (2.38) will cause significant numerical difficulties close to the contact line since in that region $h_{23} - h_{12} \to 0$. To overcome this problem, we multiply by $h_{23} - h_{12}$, and thus, the corresponding weak forms, after applying the divergence theorem, become

$$\int_0^{x_c}\left[(h_{23} - h_{12})c_{2,t} + c_{2,x}\int_{h_{12}}^{h_{23}} u_2 dz + \beta_{c2c23} J_{c2c23} + \beta_{c2c12} J_{c2c12} + (h_{23} - h_{12})J_2\right]\phi_i dx + \int_0^{x_c}\frac{(h_{23} - h_{12})c_{2,x}}{Pe_{c2}}\phi_i x dx - \left[\frac{(h_{23} - h_{12})c_{2,x}}{Pe_{c2}}\right]_0^{x_c} = 0, \quad \text{(C10)}$$

$$\int_0^{x_c}\left[\left((h_{23} - h_{12})m_{2,t} + m_x\int_{h_{12}}^{h_{23}} u_2 dz - (h_{23} - h_{12})J_2\right)\phi_i + \frac{(h_{23} - h_{12})m_{2,x}}{Pe_{m2}}\phi_{i_x}\right]dx - \left[\frac{(h_{23} - h_{12})m_{2,x}}{Pe_{m2}}\right]_0^{x_c} = 0. \quad \text{(C11)}$$

Downloaded 22 Dec 2011 to 129.31.211.195. Redistribution subject to AIP license or copyright; see http://pof.aip.org/about/rights_and_permissions

APPENDIX D: MAPPING OF THE PHYSICAL ONTO THE COMPUTATIONAL DOMAIN

The physical domain consists of two parts, one upstream of the contact line and one downstream of it. During the spreading process, the contact line moves, and therefore, the physical domain changes with time. In order to map the transient physical domain, (x,t), onto a computational domain fixed in time, (η,τ), we use the following set of algebraic equations:

$$x = \eta x_c \text{ for } 0 \le \eta \le 1, \tag{D1}$$

$$x = \frac{A + B(x_c - x_\infty)}{B(B-1)}\eta^2 - \frac{3A + B(B+2)(x_c - x_\infty)}{B(B-1)}\eta + \frac{2A + B(2Bx_c - (B+1)x_\infty)}{B(B-1)} \text{ for } 1 \le \eta \le 2, \tag{D2}$$

$$\text{and } \tau = t, \tag{D3}$$

where $A = x_c/N_1$, $B = 1/N_2$, and N_1, N_2 denote the number of grid elements in domains 1 and 2, respectively. The physical domain for $0 \le x \le x_c$ is mapped onto $0 \le \eta \le 1$ while the one for $x \ge x_c$ is mapped onto $1 \le \eta \le 2$. The mapping we use for the second domain can guarantee an optimum distribution of nodes in the physical domain at all times during the simulation presented in this paper. The derivatives that arise in the evolution equations also have to be rewritten in terms of the new variables,

$$\partial_t = \partial_\tau - \frac{d\eta}{dt}\partial_\eta, \quad \partial_x = \frac{\partial \eta}{\partial x}\partial_\eta, \tag{D4}$$

and Eq. (D4) is used to replace the corresponding terms in the weak form of the governing equations presented above as well as in the corresponding boundary conditions.

Each computational domain is discretized using 150 elements in all the computations presented in this paper; numerical checks showed that increasing the number of elements further led to negligible changes. In all the simulations presented below, the surfactant mass conservation is satisfied within 0.01%.

[1]W. D. Harkins, *The Physical Chemistry of Surface Films* (Reinhold, New York, 1952).
[2]P. R. Pujado and L. E. Scriven, "Sessile lenticular configurations: Translationally and rotationally symmetric lenses," J. Colloid Interface Sci. **40**, 82 (1972).
[3]N. D. Dipietro, C. Huh, and R. G. Cox, "The hydrodynamics of the spreading of one liquid on the surface of another," J. Fluid Mech. **84**, 529 (1978).
[4]N. D. Dipietro and R. G. Cox, "The containment of an oil slick by a boom placed across a uniform stream," J. Fluid Mech. **96**, 613 (1980).
[5]M. Foda and R. G. Cox, "The spreading of thin liquid films on a water-air interface," J. Fluid Mech. **101**, 33 (1980).
[6]D. P. Hoult, "Oil spreading on sea," Annu. Rev. Fluid Mech. **4**, 341 (1972).
[7]S. Berg, "Marangoni-driven spreading along liquid-liquid interfaces," Phys. Fluids **21**, 032105 (2009).
[8]J.-F. Joanny, "Wetting of a liquid substrate," PCH, PhysicoChem. Hydrodyn. **9**, 183 (1987).
[9]J. G. E. Fraaije and A. M. Cazabat, "Dynamics of spreading on a liquid substrate," J. Colloid Interface Sci. **133**, 452 (1989).
[10]J. J. Kriegsmann and M. J. Miksis, "Steady motion of a drop along a liquid interface," SIAM J. Appl. Math. **64**, 18 (2003).
[11]R. V. Craster and O. K. Matar, "On the dynamics of liquid lenses," J. Colloid Interface Sci. **303**, 503 (2006).
[12]L. W. Schwartz and R. R. Eley, "Simulation of droplet motion on low-energy and heterogeneous surfaces," J. Colloid Interface Sci. **202**, 172 (1998).
[13]D. A. Edwards, H. Brenner, and D. T. Wasan, *Interfacial Transport Processes and Rheology* (Butterworth-Heinemann, New York, 1991).
[14]E. A. Van Nierop, A. Adjari, and H. A. Stone, "Reactive spreading and recoil of oil on water," Phys. Fluids **18**, 038105 (2006).
[15]V. Bergeron and D. Langevin, "Monolayer spreading of polydimethysiloxne oil on surfactant solutions," Phys. Rev. Lett. **76**, 3152 (1996).
[16]P. Joos and J. Van Nunsel, "Spreading of aqueous surfactant solutions on organic liquids," J. Colloid Interface Sci. **106**, 161 (1984).
[17]T. F. Svitova, H. Hoffmann, and R. M. Hill, "Trisiloxane surfactants: Surface/interfacial tension dynamics and spreading on hydrophobic surfaces," Langmuir **12**, 1712 (1996).
[18]T. Stoebe, Z. Lin, R. M. Hill, M. D. Ward, and H. T. Davis, "Enhanced spreading of aqueous films containing ethoxylated alcohol surfactants on solid substrates," Langmuir **13**, 7270 (1997).
[19]T. Stoebe, Z. Lin, R. M. Hill, M. D. Ward, and H. T. Davis, "Superspreading of aqueous films containing trisiloxane surfactant on mineral oil," Langmuir **13**, 7282 (1997).
[20]T. F. Svitova, R. M. Hill, Y. Smirnova, A. Stuermer, and G. Yahukov, "Wetting and interfacial transitions in dilute solutions of trisiloxane surfactants," Langmuir **14**, 5023 (1998).
[21]T. F. Svitova, R. M. Ill, and C. J. Radke, "Spreading of aqueous dimethyldidodecylammonium bromide surfactant droplets over liquid hydrocarbon substrates," Langmuir **15**, 7392 (1999).
[22]A. Chauhan, T. F. Svitova, and C. J. Radke, "A sorption-kinetic model for surfactant-driven spreading of aqueous drops on insoluble liquid substrates," J. Colloid Interface Sci. **222**, 221 (2000).
[23]T. F. Svitova, R. M. Hill, and C. J. Radke, "Spreading of aqueous trisiloxane surfactant solutions over liquid hydrophobic substrates," Langmuir **17**, 335 (2001).
[24]R. Stocker and J. W. M. Bush, "Spontaneous oscillations of a sessile lens," J. Fluid Mech. **583**, 465 (2007).
[25]F. Sebba, *Macrocluster Gas-Liquid and Biliquid Foams and Their Biological Significance*, ACS Symposium Series Vol. **9** (American Chemical Society, Washington, DC, 1975), pp. 18–39.
[26]G. Karapetsas, R. V. Craster, and O. K. Matar, "On surfactant-enhanced spreading and superspreading of liquid drops on solid surfaces," J. Fluid Mech. **670**, 5 (2011).
[27]O. K. Matar and R. V. Craster, "Dynamics of surfactant-assisted spreading," Soft Matter **5**, 3801 (2009).
[28]C. Maldarelli, "On the microhydrodynamics of superspreading," J. Fluid Mech. **670**, 1 (2011).
[29]B. D. Edmonstone, R. V. Craster, and O. K. Matar, "Surfactant-induced fingering phenomena beyond the critical micelle concentration," J. Fluid Mech. **564**, 105 (2006).
[30]R. J. Hunter, *Foundations of Colloid Science* (Oxford University Press, New York, 1991).
[31]C. J. W. Breward and P. D. Howell, "Straining flow of a micellar surfactant solution," Eur. J. Appl. Math. **15**, 511 (2004).
[32]A. Sheludko, "Thin liquid films," Adv. Colloid Interface Sci. **1**, 391 (1967).
[33]D. P. Gaver III and J. B. Grotberg, "The dynamics of a localized surfactant on a thin film," J. Fluid Mech. **213**, 127 (1990).
[34]O. E. Jensen and J. B. Grotberg, "The spreading of heat or soluble surfactant along a thin film," Phys. Fluids A **5**, 58 (1993).

Downloaded 22 Dec 2011 to 129.31.211.195. Redistribution subject to AIP license or copyright; see http://pof.aip.org/about/rights_and_permissions